buildings

MDPI

Article

Hygrothermal and Thermal Comfort Performance of Bamboo–Plastic Bricks in Tropical Informal Settlements: Multi-Scalar Simulation in BaSECo, Manila

Liza Fahmy [1,*], Mohamed Aboeloyoon [1,2] and Giuliana Iannaccone [1]

[1] Department of Architecture, Built Environment and Construction Engineering (ABC), Politecnico di Milano, Via Ponzio 31, 20133 Milan, Italy; mohamedaboeloyoonahmed@gmail.com (M.A.); giuliana.iannaccone@polimi.it (G.I.)
[2] ARC Centre for Next-Gen Architecture Manufacturing, Adelaide University, Adelaide, SA 5005, Australia
* Correspondence: lizahfahmy@gmail.com

Abstract

Residents of informal settlements in Manila, Philippines, experience severe indoor heat stress and hygrothermal discomfort compounded by socioeconomic precarity. This paper evaluates a modular Bamboo–Plastic Brick (BPB), combining bamboo culms with 3D-printed recycled plastic frames, as a climate-responsive alternative to conventional Concrete Hollow Blocks (CHBs) for tropical informal housing. A multi-scalar computational assessment was conducted to evaluate its performance: steady-state 2D thermal analysis (THERM) evaluated heat flow and thermal bridging at the brick and brick-to-brick connection scale; dynamic hygrothermal simulation (WUFI) assessed moisture and heat transfer through the wall cross-section; and single-zone dynamic thermal simulation (IESVE) quantified indoor thermal comfort and humidity in a BaSECo residential unit. At the wall scale, the BPB's stratigraphy provides effective hygrothermal defense: while the exterior face sustains seasonal moisture accumulation during the monsoon, the interior surface maintains a zero mold growth index year-round. At the zone scale, BPB maintains indoor relative humidity within the optimal 40–60% range for 4345 h (50% of the year), at low ventilation (1 ACH), significantly outperforming the CHB baseline of 29%. However, achieving adaptive thermal comfort requires maximizing natural ventilation to 10 ACH, at which point all envelope systems achieve thermal comfort for approximately 50% of the year. This reveals a fundamental operational trade-off in tropical passive design: the ventilation rates required for thermal comfort inherently compromise indoor humidity control, and vice versa. It is concluded that the BPB shows promising hygrothermal and thermal performance as an alternative to CHB when deployed with maximized natural ventilation, with its circular fabrication workflow addressed in a companion study.

Keywords: bamboo–plastic brick; hygrothermal simulation; adaptive thermal comfort; natural ventilation; mold growth risk; thermal mass; informal settlements; circular economy

Check for updates

Academic Editor: Antonio Caggiano

Received: 12 August 2026
Revised: 21 September 2026
Accepted: 8 October 2026
Published: 22 October 2026

Copyright: © 2026 by the authors. Licensee MDPI, Basel, Switzerland. This article is an open access article distributed under the terms and conditions of the Creative Commons Attribution (CC BY) license.

1. Introduction

Asian countries are currently experiencing unprecedented rates of urbanization, driven by uneven regional economic development and persistent rural-to-urban migration. The Philippines strongly exemplifies this trajectory in its capital, Manila. Driven by rapid economic growth but lacking the physical infrastructure and affordable housing to support the influx of migrants, Manila currently carries over 1.6 million informal settlers, comprising

nearly a third of the city's total population [1]. This severe housing crisis forces residents into highly vulnerable, spontaneously built communities, exposing them to compounding socioeconomic and environmental risks, among which the BaSECo compound is a critical case.

1.1. The Dual Crisis in BaSECo: Vulnerability of the Built Environment and the Residents

Situated on a sensitive shoreline within Manila, the BaSECo compound exemplifies the intersection of tropical climate extremes and acute socioeconomic precarity. Lacking secure formal housing, residents live in a constant state of vulnerability that stifles economic productivity and human potential [2]. The settlement is highly exposed to intense solar radiation and severe moisture levels that frequently reach 100% relative humidity [3]. As a result, inhabitants are subjected to a dual crisis: persistent socioeconomic marginalization [4] and severe physiological heat stress from chronic indoor overheating and humidity exposure [5].

Historically, government and non-governmental housing initiatives in these vulnerable areas have relied heavily on conventional industrialized materials, predominantly Concrete Hollow Blocks (CHBs), steel, and corrugated metal [6]. While intended to provide structural permanence, these materials fundamentally exacerbate the environmental vulnerability of the built environment. From a building physics perspective, concrete structures in tropical climates suffer from high thermal mass that traps heat during the day and releases it at night, causing severe indoor temperature fluctuations and chronic thermal discomfort [7]. Furthermore, these conventional materials present poor moisture buffering capacities, leading to humidity accumulation within the building envelope [8]. The resulting degradation of the indoor air quality poses significant risks to the respiratory health of occupants [9].

Beyond these physiological and hygrothermal impacts, the homogenization of the built environment through concrete and steel has led to a steep decline in the use of natural materials and traditional construction methods. This shift not only contributes significantly to global carbon emissions and resource depletion [10] but also erodes the distinctive cultural identities embedded in vernacular architecture [11]. As homes become less reflective of local cultures and environments, there is a critical need to transition away from concrete dependency in sensitive ecological contexts toward sustainable, climate-responsive building solutions that address both the physiological comfort and the cultural identity of occupants.

1.2. Research Background

To contextualize the proposed BPB system within the existing body of knowledge, the background literature addresses three intersecting areas: the hygrothermal potential of natural bamboo as a low-carbon alternative to concrete and the ecological costs of its industrial standardization; the morphological irregularities of raw bamboo culms that create bottlenecks in structural standardization and computational building physics modeling; and the emergence of hybrid digital fabrication systems that combine additive manufacturing with recycled plastic waste. The structural and circular economy dimensions of this hybrid system are developed in a companion study [12], while this paper focuses on their hygrothermal performance in tropical informal housing.

1.2.1. The Bamboo Paradigm: Material Performance and Ecological Costs of Engineered Bamboo

Among high-performance bio-based materials, bamboo has emerged as a highly viable alternative for structural applications in the Global South. As a raw material, round bamboo culms exhibit rapid renewability, high carbon sequestration capacity, and exceptional

tensile strength [13]. The culm's naturally optimized tubular form provides an impressive strength-to-weight ratio that enables it to bear substantial structural loads and stresses, and its inherent elasticity allows for efficient energy absorption [14]. These properties make bamboo a highly resilient material for load-bearing frameworks in low-rise construction, rivalling, and in some metrics exceeding, the performance of structural steel [15].

From a building physics perspective, highly porous biomaterials like bamboo offer superior hygrothermal performance compared to conventional concrete. While concrete exhibits high thermal mass and poor moisture buffering [7,8], natural bamboo actively regulates indoor humidity through moisture absorption and desorption, significantly mitigating the physiological heat stress experienced in tropical climates [16].

A systematic review of bamboo envelope performance under hot and humid tropical conditions confirms these hygrothermal advantages while also noting that thermal comfort in naturally ventilated buildings remains primarily dependent on ventilation strategy rather than envelope material alone [17].

Despite these natural advantages, marginalized communities often view traditional bamboo building methods unfavorably. Studies indicate that inhabitants frequently reject local bamboo traditions, perceiving the raw material as temporary and unsafe. This preference is driven by complex social representations; residents tend to choose less sustainable conventional materials for their symbolic value such as perceived status and permanence rather than for their actual performance in providing comfort or overall dwelling quality [18]. In response to this social resistance and the demand for standardized aesthetics, the architectural industry often defaults to heavily engineered structural bamboo products. To overcome the plant's natural heterogeneity, manufacturers frequently rely on densification, a thermo-mechanical process that compresses the culms under high heat and pressure to enhance mechanical strength and create uniform structural profiles [19]. While engineered panels successfully transform the raw material into predictable, flat geometries, the intensive industrial processes required such as shredding, hot-pressing, and the use of synthetic adhesives substantially increase the material's embodied carbon and diminish its fundamental ecological benefits [20,21].

1.2.2. The Geometric Challenge: Limitations in Standardizing Raw Culms

The fundamental barrier to utilizing raw bamboo in performance-driven architecture lies in its lack of computational predictability. In hygrothermal modeling and envelope simulations, reliable calculations rely on standardized geometries and uniform material interfaces. Because raw culms naturally vary in taper, wall thickness, and internode spacing [22,23], they defy the standardized Cartesian logic required by modern modeling software. Each individual culm behaves uniquely under mechanical and thermal loads, making system-wide performance highly difficult to predict and simulate [24].

To circumvent the natural heterogeneity, building performance simulations frequently rely on significant geometric and material idealizations. Standard energy modeling engines are inherently designed to calculate 1D or 2D heat and moisture transfer through planar orthogonal assemblies [25]. Because raw bamboo culms present significant geometric irregularities that complicate computational modeling [24], their morphology must be digitally abstracted into simplified flat layer equivalents for hygrothermal analysis. These necessary abstractions yield reliable baseline data for overall thermal resistance but inherently risk masking the localized thermal bridging, air leakage, and moisture infiltration that occur at the irregular connection points of real-world physical assemblies [26].

The discrepancy between idealized computational models and physical reality is most pronounced at structural connection points. Traditional bamboo joinery methods such as manual lashing, bolting, or artisanal carving rely on highly variable craftsmanship that

introduces chaotic geometries into the building envelope [27]. From a building physics perspective, these irregular connections result in uncontrolled dimensional tolerances, creating significant pathways for convective heat loss, thermal bridging, and moisture infiltration that cannot be accurately captured by simplified 1D or 2D simulations [8,28]. Consequently, integrating raw bamboo into performance-driven standardized architectural systems without resorting to ecologically damaging densification requires a novel joinery paradigm. This system must act as a geometric mediator, physically adapting to the heterogeneous morphology of the raw culm while simultaneously providing a standardized, predictable interface that aligns with both digital hygrothermal algorithms and modular construction requirements [29].

1.2.3. Digital Fabrication and the Circular Economy: State-of-the-Art in Hybrid Systems

To overcome the limitations of heterogeneous natural materials, the integration of Digital Fabrication (Dfab) and Additive Manufacturing (AM) offers a critical technological bridge. Recent studies demonstrate that pairing parametric design with 3D printing allows for the creation of customized, adaptive joints that effectively compensate for the dimensional inconsistencies of natural bamboo culms [12]. By combining material intelligence with these modern manufacturing techniques, researchers have successfully standardized bamboo into cohesive, smart structural units [30]. This hybridization directly addresses the uncontrolled dimensional tolerances responsible for the thermal bridging and moisture infiltration discussed previously.

The urgency of transitioning to recycled polymers is particularly acute in the Global South, where rapid urbanization often outpaces waste management infrastructure. In the Philippines, it is estimated that over 2.7 million tons of plastic waste are generated annually [31]. Within the dense informal settlements of Manila, such as the BaSECo compound, the accumulation of plastic pollution contributes to severe environmental degradation. By utilizing recycled polymers, particularly extruded plastic waste, as the primary material for 3D-printed connections, architectural systems can simultaneously divert significant volumes of pollution from these vulnerable local ecosystems [32]. Real-world initiatives such as Plastic Odyssey have demonstrated the practical feasibility of processing locally sourced plastic waste into functional components in informal contexts [33], while recent research in Large-Format Additive Manufacturing (LFAM) further validates the architectural potential of such upcycled materials [32].

Beyond material innovation, deploying these systems in informal contexts necessitates a fundamental shift in the manufacturing paradigm. Centralized, industrialized production models often fail to benefit marginalized communities economically and contribute heavily to construction-related emissions. In response, the concept of decentralized production through localized micro-factories has gained significant traction as a strategy for resilient urban development [34]. By embedding small-scale, digitally equipped fabrication hubs directly within a settlement, communities are empowered to utilize local biomaterials and recovered plastic waste to manufacture their own architectural components [35]. This approach establishes a localized circular economy that provides residents with technical skills, autonomy over their built environment, and vital streams of income [36]. While the design workflow and circular production framework for such systems are developed in a companion study [12], their hygrothermal performance in tropical informal contexts remains unaddressed in the literature.

1.3. Research Gap, Objectives and Questions

1.3.1. The Research Gap

While the existing literature validates bamboo as a sustainable material and demonstrates the structural potential of 3D-printed joints and circular micro-factories [12], a critical intersection remains unexplored. Current studies focus predominantly on the structural rationalization of these assemblies. There is a distinct lack of performance-based evidence regarding the hygrothermal behavior of hybrid bamboo–plastic systems in dense, tropical urban environments. Specifically, it remains unverified whether a modular Bamboo–Plastic Brick (BPB) can thermally and hygroscopically outperform conventional Concrete Hollow Blocks (CHBs) to mitigate physiological heat stress in informal settlements like BaSECo.

1.3.2. Research Objectives and Questions

The primary goal of this research is to evaluate the hygrothermal and thermal performance of the BPB system as a sustainable, climate-responsive alternative to conventional construction in Manila. Specifically, this study aims to:

(1) Characterize the material and hygrothermal properties of the hybrid BPB assembly to establish accurate baseline data for computational building physics models.
(2) Simulate and compare the long-term hygrothermal performance of the BPB system against standard CHB construction, assessing heat transfer and moisture buffering under tropical climate conditions, and asking whether the BPB can thermally and hygroscopically outperform CHB to mitigate physiological heat stress in BaSECo.
(3) Quantify improvements in indoor thermal comfort and humidity conditions, examining under what passive ventilation conditions the BPB achieves simultaneous thermal comfort and optimal humidity control and what the implications are for tropical passive design strategy.
(4) Situate the BPB performance findings within the broader circular economy and digital fabrication framework developed in companion studies [12], demonstrating the holistic regenerative potential of the system.

2. Materials and Methods

A multi-scalar computational workflow was employed to evaluate the hygrothermal and thermal performance of the Bamboo–Plastic Brick (BPB) against conventional Concrete Hollow Blocks (CHBs) across three distinct physical scales (Figure 1). First, steady-state 2D thermal analysis evaluated heat flow and thermal bridging at the brick and brick-to-brick connection scale. This analysis used THERM (Version 7.8), developed by Lawrence Berkeley National Laboratory (LBNL, Berkeley, CA, USA). Second, dynamic hygrothermal simulations assessed long-term moisture transfer, condensation risk, and mold growth at the wall cross-section scale under tropical climate conditions. These simulations used WUFI® Pro (Version 6; Fraunhofer Institute for Building Physics IBP, Holzkirchen, Germany). Finally, single-zone dynamic thermal simulationquantified indoor operative temperatures and thermal comfort in a representative BaSECo residential unit. This simulation used the Integrated Environmental Solutions Virtual Environment (IESVE, Version 2023; Integrated Environmental Solutions Limited, Glasgow, UK). The material characterization, boundary conditions, and simulation parameters for each scale are detailed in the following subsections.

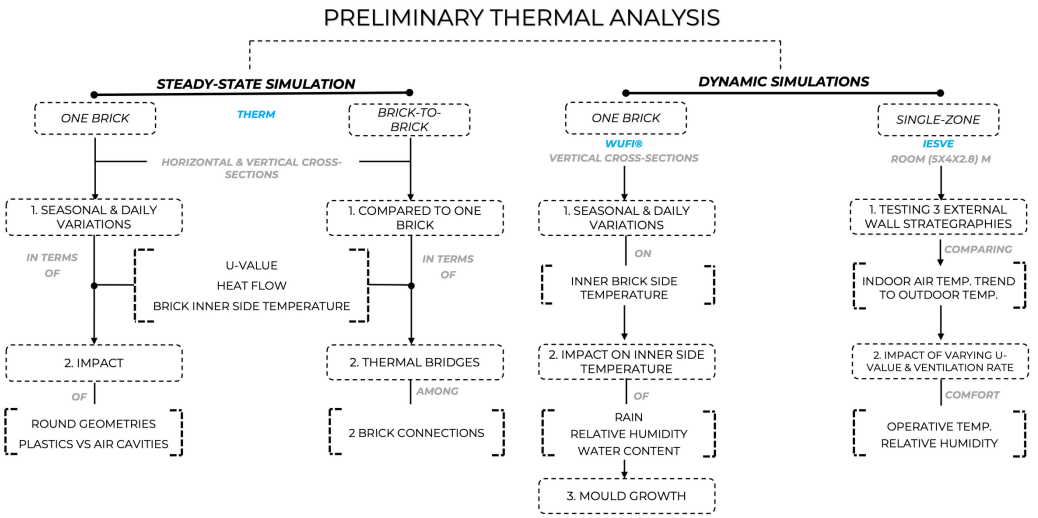


Figure 1. Methodological flowchart detailing the multi-scalar simulation workflow, progressing from steady-state 2D thermal analysis (THERM) at the brick scale, to dynamic hygrothermal wall assessment (WUFI) at the wall cross-section scale, and single-zone thermal comfort evaluation (IESVE) at the residential unit scale.

2.1. Material Characterization and BPB Assembly Profile

The Bamboo–Plastic Brick (BPB), developed and described in detail in [12], is a modular building component combining natural bamboo culms with 3D-printed recycled plastic connectors for local fabrication within informal settlements. This study focuses exclusively on evaluating the dynamic thermal and hygrothermal performance of the resulting building envelope; the physical fabrication workflow and structural assembly are addressed in [12].

Accurate evaluation of heat and moisture transfer required abstracting the physical geometry of the BPB into functional layers suitable for computational simulation. The assembly consists of natural bamboo culms integrated within a 3D-printed recycled plastic (polyethylene/PET) frame (Figure 2a), enclosed by ply-bamboo boards on both faces (Figure 2b). The 3D-printed plastic frames serve a dual function: accommodating the morphological irregularities of the raw bamboo culms while providing a standardized, planar surface for the secure attachment of the enclosing boards (Figure 2c). Internally, the assembly features distinct air cavities dictated by the round geometry of the bamboo and the enclosing plastic frame.

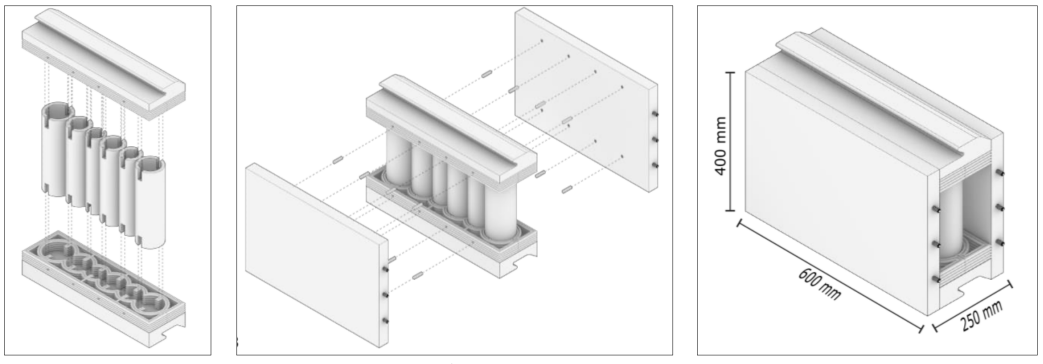


Figure 2. Design and assembly scheme of the Bamboo–Plastic Brick (BPB) modular unit: (**a**) exploded view of the internal natural bamboo culms and the top/bottom 3D-printed recycled plastic frames; (**b**) integration of the external ply-bamboo enclosing boards and connecting hardware; and (**c**) the fully assembled modular unit detailing the overall macroscopic dimensions (600 mm × 400 mm × 250 mm). The schematic identifies the primary structural and functional layers defined for the subsequent thermal and hygrothermal computational models.

For the comparative baseline, a standard Concrete Hollow Block (CHB) assembly typical of the prevalent construction in the BaSECo compound was defined (Figure 3). The specific thermophysical parameters, boundary conditions, and geometric profiles required for each simulation scale are detailed in their respective sections below.

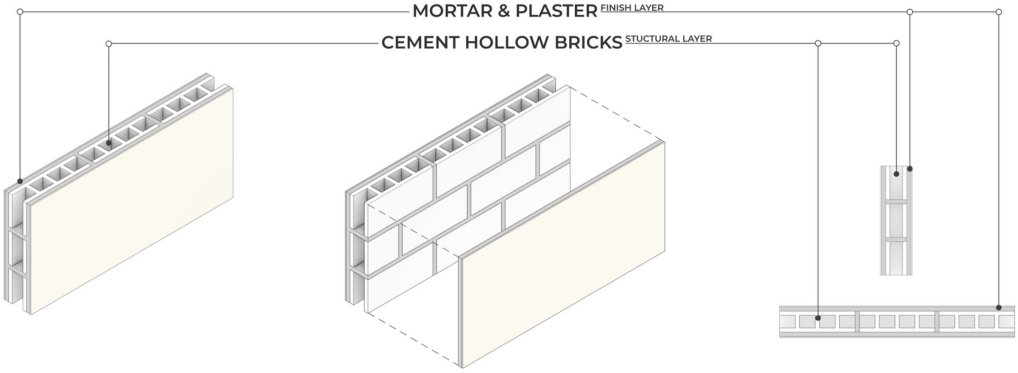


Figure 3. Schematic of the standard Concrete Hollow Block (CHB) baseline assembly representing prevalent construction in the BaSECo compound. The diagram details the primary material layers from outside to inside: external screed, cement render, hollow concrete block with internal air cavity, cement render, and internal plaster finish.

All thermophysical and hygrothermal material properties were sourced from validated published literature and standard material databases rather than experimentally measured from the proposed BPB assembly. This approach is consistent with standard computational building physics methodology for novel material systems in pre-prototype stages. Thermal properties for the steady-state analysis were taken from standard material databases (Section 2.2.2), and hygrothermal properties for the dynamic analysis were assigned from the WUFI built-in material library (Section 2.3.1). The only exception is the water vapour diffusion resistance factor of the ply-bamboo boards (μ = 1392.8), sourced from Huang et al. [37,38]. Natural bamboo properties exhibit species-dependent variability, and this factor has been identified as the most critical parameter influencing RH simulation outcomes [37,38]. This variability represents an inherent uncertainty in the simulation results, which should therefore be interpreted as indicative of performance potential rather than definitive predictions.

2.2. Steady-State Thermal Analysis (THERM)

A steady-state 2D heat transfer analysis was conducted to evaluate the thermal transmittance (U-value) and identify potential thermal bridges within the Bamboo–Plastic Brick (BPB). This phase utilized the finite-element heat transfer analysis software THERM (Version 7.8), developed by the Lawrence Berkeley National Laboratory (LBNL). Because THERM presents inherent limitations in natively meshing perfectly round geometries, an intermediate parametric workflow was developed. Grasshopper, within Rhinoceros 3D (Version 7; Robert McNeel & Associates, Seattle, WA, USA), was employed to discretize the circular cross-sections of the bamboo culms into high-resolution polygonal meshes before exporting them to the THERM environment. The visual programming workflow is detailed in Appendix A.

2.2.1. Cross-Sectional Profiles

The steady-state analysis was divided into two primary scopes, ensuring the heterogeneity of the hybrid assembly was accurately captured:

1. Single-Brick Analysis: Individual brick performance was evaluated using one vertical cross-section (A-A) representing the core wall assembly, alongside two horizontal

cross-sections. The horizontal profiles included the top bonding zone where the 3D-printed plastic adheres to the bamboo (B-B), and the typical mid-section where the internal air cavities interface with the bamboo culms (C-C) (Figure 4a).

2. Brick-to-Brick Connection: Thermal bridging effects at the assembly joints were examined following the same procedural logic. This scope included a vertical cross-section of the stacking connection (D-D), as well as two horizontal cross-sections detailing the lateral interfaces between the printed plastic plates, air cavities, and adjacent bamboo culms (E-E and F-F) (Figure 4b).

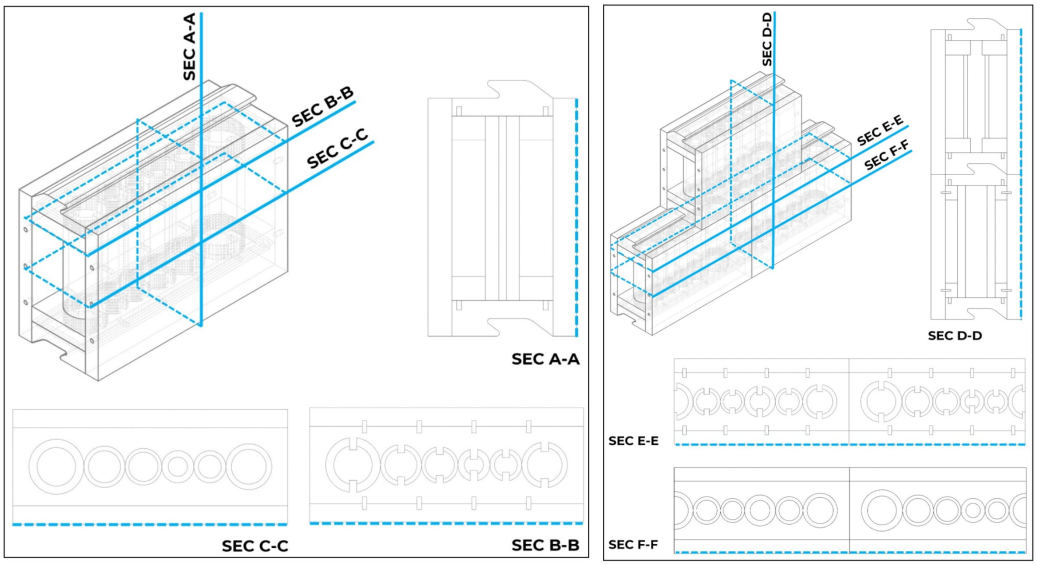


Figure 4. Cross-sections tested in THERM: (**a**) single-brick cross-sections, highlighting the vertical profile (A-A) and horizontal variations across the bonding zone (B-B) and the typical bamboo culm cross-section (C-C); (**b**) brick-to-brick cross-sections, detailing the vertical stacking connection (D-D) and horizontal lateral joints (E-E, F-F). Blue dashed lines mark the section cut positions; circles represent the bamboo culms in the horizontal sections.

2.2.2. Boundary Conditions and Material Properties

To simulate critical peak thermal stress conditions, boundary conditions were extracted from the EnergyPlus Weather File (EPW) for Manila NCR, Philippines, sourced via Climate.OneBuilding.org [3]. External temperatures were mapped for peak daytime and nocturnal hours at noon (12:00) and midnight (00:00) during both the summer solstice (21 June) and winter solstice (21 December).

The indoor temperature setpoint was fixed at 22 °C, representing the lower threshold of the predicted thermal comfort range for the Philippines (22 °C to 26 °C) [39]. This maximized the temperature differential between the interior and exterior environments, establishing a critical peak thermal stress scenario. Surface air film resistances were defined in accordance with the ISO 10077-2 standard [40], applying 0.13 m^2.K/W for the internal surface R_{SI} and 0.04 m^2.K/W for the external surface R_{SE}. Internal air cavities were modelled following the standard's numerical method for frames. The resulting environmental boundary conditions and the thermophysical material properties are summarized in Tables 1 and 2. All material properties were sourced from the ASHRAE Handbook of Fundamentals and the LBNL THERM material database [28,41].

Table 1. Environmental boundary conditions applied for steady-state thermal analysis.

Season	Date	Time	External Temperature (°C)	Internal Setpoint (°C)
Summer	21 June	12:00	32.5	22
		00:00	27.5	
Winter	21 December	12:00	29.9	22
		00:00	28.2	

Table 2. Layer thicknesses and thermophysical properties of the BPB assembly components applied in the steady-state thermal analysis.

Material Layer (Outside to Inside)	Thickness m	Thermal Conductivity, λ W/(m.K)	Emissivity, ε
Ply-bamboo board (Exterior)	0.040	0.190	0.9
Air cavity	0.025	(per ISO 10077-2)	0.9
Bamboo culm wall	0.015	0.176	0.9
Air cavity (bamboo culm interior)	0.090	(per ISO 10077-2)	0.9
Bamboo culm wall	0.015	0.176	0.9
Air cavity	0.025	(per ISO 10077-2)	0.9
Ply-bamboo board (Interior)	0.040	0.190	0.9
Structural Frame Component			
Recycled Polyethylene (3D Print)	0.025	0.500	0.9

2.3. Dynamic Hygrothermal Wall Cross-Section Simulation (WUFI)

2.3.1. Simulation Setup and Initial Conditions

A dynamic hygrothermal analysis was conducted using WUFI® Pro 6 to evaluate the coupled heat and moisture transfer through the Bamboo–Plastic Brick (BPB) under transient environmental conditions. Recognizing the inherent limitations of steady-state analysis that cannot account for latent heat effects, rain infiltration, or moisture accumulation, this 1D transient simulation quantified the hygrothermal performance of the multilayered assembly over a complete meteorological year.

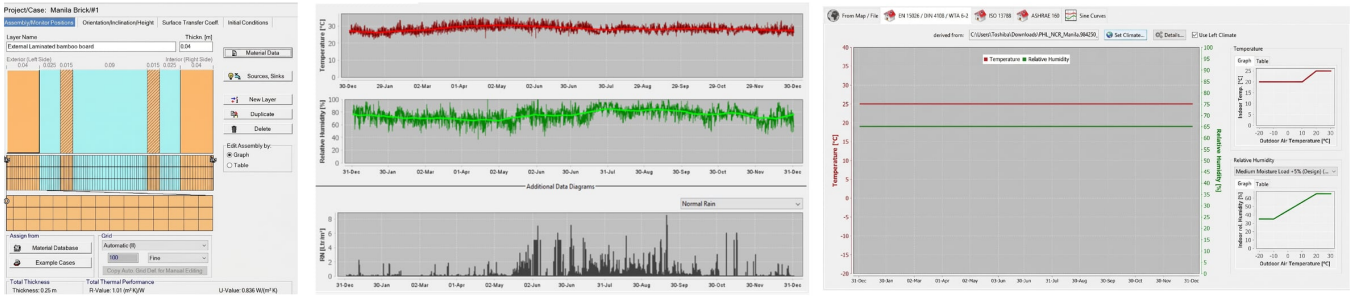
Establishing a robust baseline for the transient simulation required defining specific initial conditions for the modeled components prior to the one-year evaluation period. In accordance with the EN 15026 standard, a constant initial relative humidity of 80% was applied uniformly across all assembly layers [42]. From this boundary, the software derived the initial water content using the specific moisture storage functions of the evaluated materials [43,44]. The initial component temperature was fixed at 20 °C as a conventional starting value consistent with standard WUFI simulation practice [25]. The influence of this initial temperature on annual results is limited, since the thin bamboo layers reach thermal equilibrium with the boundary conditions within the first hours of the simulation.

The brick layers, specifically the exterior and interior ply-bamboo boards, bamboo culm walls, and internal air cavities, were sequentially defined in the software, alongside their corresponding hygrothermal material properties. All properties were assigned from the WUFI built-in material library, except for the water vapour diffusion resistance factor (μ = 1392.8) for the ply-bamboo boards, which was sourced from Huang et al. [37,38] and is discussed further in Section 4.4.

2.3.2. Boundary Conditions and Climate Data

The dynamic simulation was configured to run for one complete meteorological year. Environmental boundary conditions for the external surface, comprising hourly air

temperature, relative humidity, solar radiation, and driving rain profiles, were imported from the EnergyPlus Weather File (EPW) for Manila, Philippines [3]. The indoor climate was then derived from the outdoor environment in accordance with the WTA Guideline 6-2 and EN 15026 standard [25,42]. The indoor environmental setpoints were fixed at 25 °C and 65% relative humidity, representing a conservative tropical indoor reference condition (Figure 5).



(**a**) (**b**) (**c**)

Figure 5. Dynamic hygrothermal simulation setup in WUFI® Pro, detailing: (**a**) the 1D multilayered component assembly of the Bamboo–Plastic Brick, showing the ply-bamboo boards (solid orange), bamboo culm walls (hatched orange), air layers (light blue), the numerical grid (lower strips), and the monitor positions at the exterior and interior surfaces (camera symbols);(**b**) the transient outdoor boundary conditions (Manila EPW), showing air temperature (red), relative humidity (green), and hourly normal rain (bars), with darker lines for hourly values and lighter lines for the smoothed trend; and (**c**) the prescribed indoor climate boundary conditions derived in accordance with EN 15026 and WTA Guideline 6-2, showing air temperature (red) and relative humidity (green). The small graphs in (c) show indoor temperature and relative humidity as functions of outdoor air temperature, using the medium moisture load +5% (design) setting.

2.3.3. Mold Growth Risk Assessment

Following the hygrothermal simulation, a post-processing biological assessment was conducted to evaluate the risk of mold growth within the organic substrates of the assembly. It used WUFI® Bio (Fraunhofer IBP, Holzkirchen, Germany) as a post-processor of the WUFI® Pro results. This assessment is critical for bio-based materials such as bamboo to ensure long-term structural integrity and indoor air quality. Four critical cross-sectional interfaces representing the contact points between the ply-bamboo boards, bamboo culm walls, and the internal air cavities were monitored (Figure 6). The evaluation used the Viitanen model [45], which classifies the probability of mold development on a seven-point index scale (MI 0–6). MI 0 means no growth. At MI 1 and MI 2, growth is visible only under a microscope. Growth at MI 2 is moderate, with coverage above 10%. By MI 3, growth is detected by eye, and thin hyphae are found under the microscope. Visible coverage exceeds 10% at MI 4. At MI 5, coverage is above 50%. MI 6 means tight coverage of 100% [45]. This index is calculated based on the localized transient temperature and relative humidity profiles, where a Mould Index (MI) below 3 is required to prevent visible surface growth.

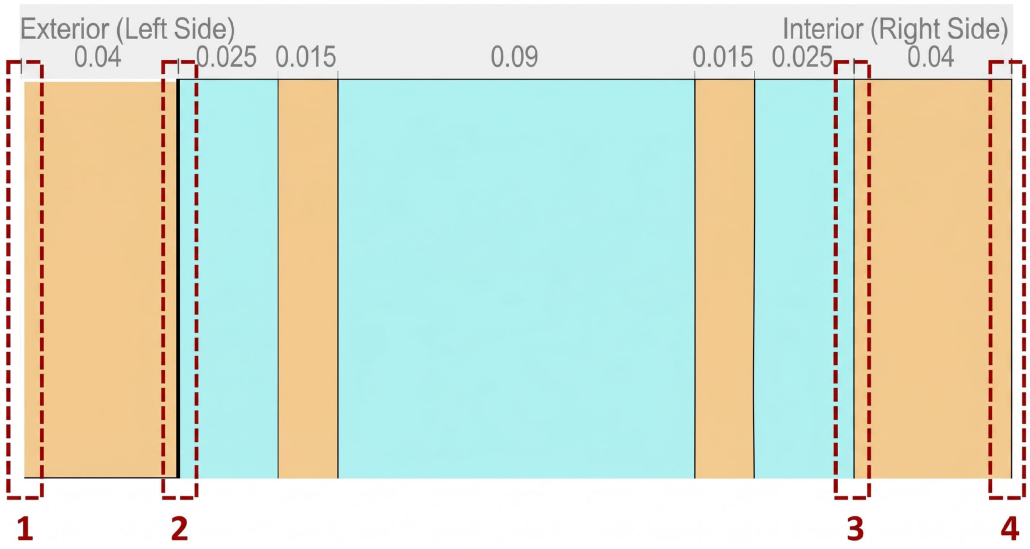


Figure 6. Critical cross-sectional interfaces monitored for mold growth risk assessment within the BPB wall assembly, identified using WUFI® Bio. Orange layers represent the bamboo-based materials and light blue layers represent the air cavities. Numbers above the assembly give the layer thicknesses (m). Red dashed boxes mark the monitored interfaces: (1) outer face of the exterior board (CS 1); (2) inner face of the exterior board (CS 2); (3) cavity-facing face of the interior board (CS 3); (4) space-facing face of the interior board (CS 4).

2.4. Thermal Zone Dynamic Simulation (IESVE)

2.4.1. Simulation Software and Computational Workflow

To bridge the gap between component-level moisture analysis and residential unit thermal performance, a single-zone dynamic thermal simulation was conducted using the Integrated Environmental Solutions Virtual Environment (IESVE, Version 2023) [46]. IESVE is an integrated suite of building physics applications linked by a single centralized data model, ensuring consistent data transfer across simulation phases. The simulation workflow used three primary modules: ModelIT to construct the 3D geometry of the thermal zone; ApacheSim to execute the dynamic thermal calculations [47]; and VistaPro (IES Virtual Environment, 2023) to extract and post-process the hourly thermal simulation results [46]. This phase evaluated a standardized single-zone model to systematically quantify the thermal performance of the BPB against the conventional CHB baseline.

2.4.2. Geometry and Model Setup

The dynamic thermal zone simulation was performed on a standardized single-zone rectangular model, which serves as a controlled baseline for evaluating the thermal performance of building envelopes. To ensure the model remained representative of local residential typologies, the zone geometry was based on documented housing units in the BaSECo area [6], where typical floor areas for social housing units (e.g., Gawad Kalinga) range between 20.0 m^2 and 24.0 m^2. Consequently, a representative 20.0 m^2 room (5.0 m in length, 4.0 m in width, and 2.8 m in height) was constructed in the ModelIT module (Figure 7a). This geometry was used to evaluate the thermal performance of the BPB against the conventional CHB assemblies, which represent the predominant construction material for these units [6]. The model included two 1.0 m^2 windows positioned on the north and east facades at a sill height of 1.5 m, yielding a total Window-to-Wall Ratio (WWR) of 4.0% consistent with the minimal fenestration observed in documented BaSECo housing typologies. To focus the analysis on passive thermal performance, the simulation assumed a fully naturally ventilated environment. As shown in the software templates (Figure 7b,c),

all active systems, specifically mechanical HVAC, auxiliary ventilation, and domestic hot water, were either defined as "none" or set to an "off continuously" operational profile [47].

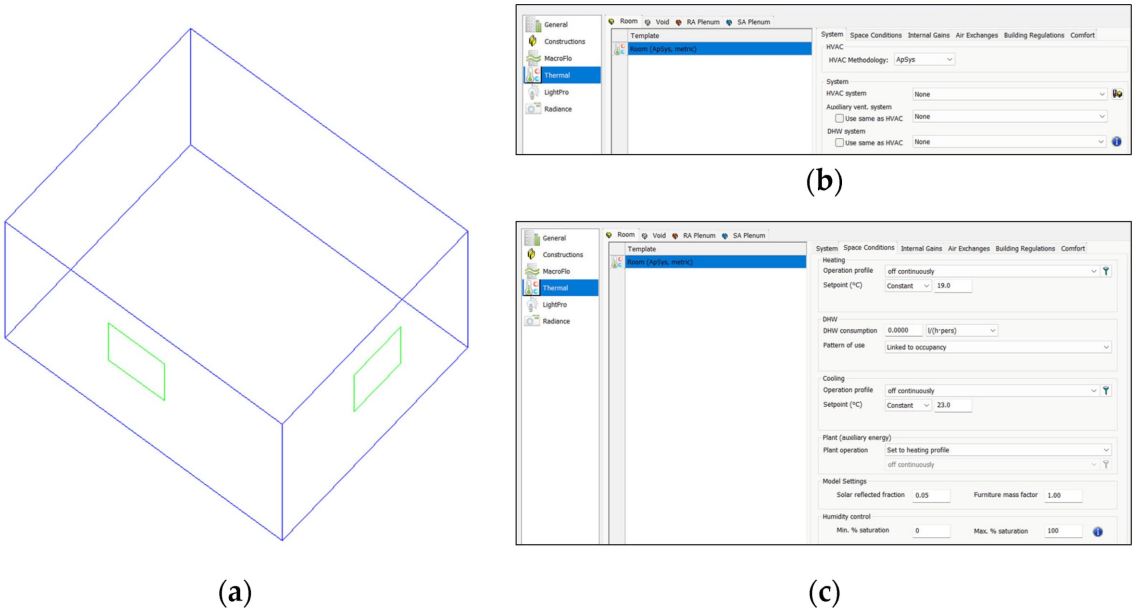


Figure 7. Representative single-zone model geometry in IESVE, detailing: (**a**) the 3D thermal zone geometry, with the zone edges in purple and the two windows in green; (**b**) the system templates set to "none"; and (**c**) the space condition profiles set to "off continuously".

2.4.3. Internal Gains

Thermal gain parameters were defined within the IESVE Internal Gains template (Figure 8a) to evaluate the impact of internal heat sources on the thermal zone's performance. An occupancy density of 10 m^2 per person was assigned, resulting in two occupants for the 20.0 m^2 model. The sensible heat gain was set at 90 W/person, and the latent heat gain was defined as 60 W/person, in accordance with ASHRAE Handbook of Fundamentals metabolic rate standards for sedentary activities [28]. The electrical load for internal appliances and lighting was modeled with a power density of 6 W/m^2 (Figure 8a) [48]. These values remained constant across all simulation scenarios to ensure a direct comparison of the building envelope's thermal response.

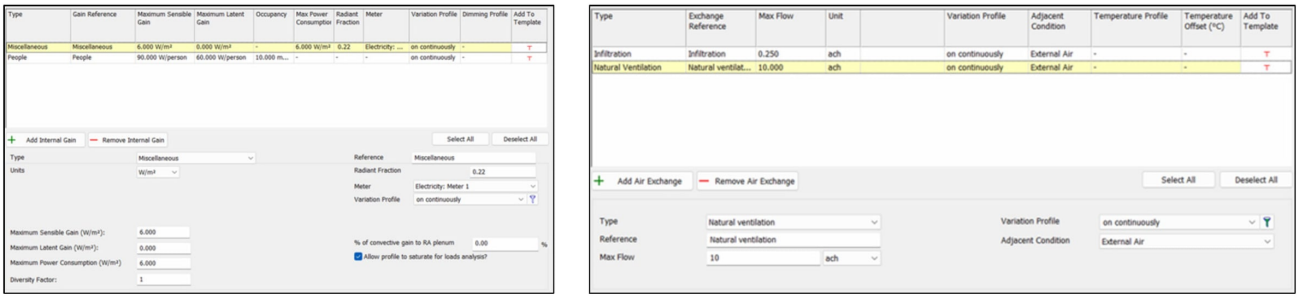


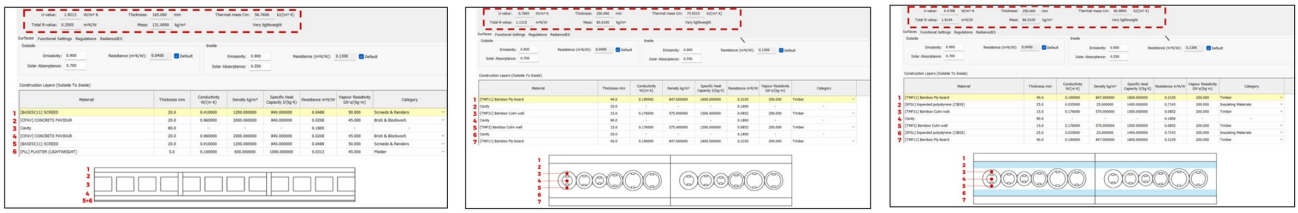
Figure 8. IESVE simulation input templates: (**a**) internal gains template, detailing the specific heat gain parameters for occupants (90 W/person sensible, 60 W/person latent) and internal appliances (6 W/m^2), and (**b**) air exchanges template, detailing the fixed infiltration rate (0.25 ACH) and the natural ventilation rate, shown here for the 10 ACH scenario. The ventilation rate was varied across the simulations scenarios (1, 5, and 10 ACH).

2.4.4. Air Exchanges: Infiltration and Ventilation Parameters

Air exchange rates within the thermal zone were defined to account for both unintended infiltration and intentional ventilation. A fixed infiltration rate of 0.25 ACH was applied across all simulation scenarios to represent the baseline envelope airtightness. The intentional ventilation rate for the baseline simulation was set at 1 ACH. This value exceeds the minimum requirement of 0.35 ACH for residential buildings per ASHRAE Standard 62.1 [49], representing a realistic conservative natural ventilation scenario for informal housing in Manila where mechanical cooling is absent. Ventilation rates of 5 ACH and 10 ACH were selected to systematically explore the full spectrum from baseline to maximum natural ventilation conditions. These configurations are detailed in the Air Exchanges template (Figure 8b).

2.4.5. Construction Template

The physical properties of the building envelope were defined within the IESVE construction database to accurately simulate thermal exchange. The model comprised six distinct construction assemblies, with the roof, floor, and windows held constant across all simulations to isolate the external walls as the sole variable under investigation. Three distinct scenarios were developed for the external walls. The first represented the existing baseline construction in BaSECo, using a standard CHB assembly with cement and screed finishes (Figure 9a). The second modeled the proposed BPB; due to software limitations regarding cylindrical geometries, the bamboo culms were approximated as alternating flat layers of bamboo and air cavities enclosed by ply-bamboo boards (Figure 9b). The third scenario enhanced the BPB model by replacing the outer air cavities with Expanded Polystyrene (EPS) insulation (Figure 9c). The stratigraphy, total thicknesses, thermal transmittances (U-values), and thermal mass capacities for all six components are summarized in Table 3.



(**a**) (**b**) (**c**)

Figure 9. Stratigraphy of the tested external wall assemblies in IESVE, detailing the layer configurations for: (**a**) the Baseline CHB; (**b**) the Standard Bamboo–Plastic Brick, with circles representing the bamboo culms and red leader lines locating layers 3 to 5 within a culm; and (**c**) the BPB with EPS Insulation, with the same culm representation as in (b) and light blue bands representing the EPS layers. In all panels, the red dashed box highlights the overall properties of the construction (U-value, total R-value, thickness, mass, and thermal mass), and red numbers link each table layer to the section schematic below.

Table 3. Thermo-physical properties and stratigraphy of the building envelope components used in the dynamic simulations.

Building Component	Material Layers (Outside to Inside)	Total Thickness mm	U-Value W/(m^2.K)	Thermal Mass kJ/(m^2.K)
1. External Wall (Baseline CHB)	Screed/Cement/Air Cavity/Cement/Screed/Plaster	165.0	1.921	56.76

Table 3. *Cont.*

Building Component	Material Layers (Outside to Inside)	Total Thickness mm	U-Value W/(m^2.K)	Thermal Mass kJ/(m^2.K)
2. External Wall (BPB Standard)	Ply-bamboo/Air Cavity/Bamboo/Air Cavity/Bamboo/Air Cavity/Ply-bamboo	250.0	0.768	73.92
3. External Wall (BPB + Insulation)	Ply-bamboo/EPS/Bamboo/Air Cavity/Bamboo/EPS/Ply-bamboo	250.0	0.479	60.98
4. Windows (Predefined)	6 mm Clear Glass/12 mm Argon/6 mm Clear Glass	24.0	1.600	-
5. Floor (Predefined)	Standardized floor layers + Screed finish	238.2	0.228	-
6. Roof (Predefined)	Standardized roof layers	-	0.180	98.75

2.4.6. Weather Data and Simulation Settings

Annual dynamic thermal simulations were executed using the ApacheSim engine within IESVE(Version 2023). Climate conditions were established via an EnergyPlus Weather (EPW) data file for NCR Manila, Philippines, directly reflecting the microclimate of the BaSECo site [3]. Simulations ran from 1 January to 31 December with a 10-min time step, yielding high-resolution transient data at six points per hour. A 30-day pre-conditioning period was implemented prior to the start date, ensuring the building envelope's thermal mass reached a realistic equilibrium before data collection began.

Seven simulations, organized into four progressive sets, systematically evaluated the wall assemblies (Figure 10):

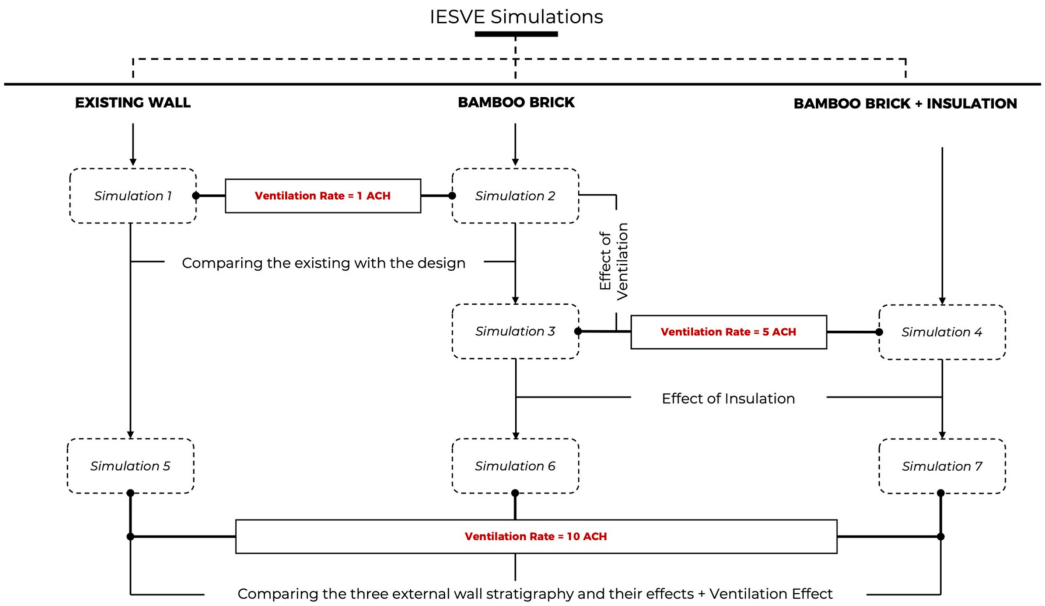


Figure 10. Logical flow of the dynamic simulation procedure, detailing the four progressive sets and seven simulation runs used to evaluate the wall assemblies. Dashed boxes represent the individual simulation runs, and red labels give the ventilation rate applied in each comparison.

1. Set 1 (Baseline Comparison): Evaluated the existing CHB wall against the standard BPB under the baseline ventilation rate of 1 ACH, comprising Simulation 1 (CHB at 1 ACH) and Simulation 2 (BPB at 1 ACH);

2. Set 2 (Ventilation Impact): Examined the thermal response of the standard BPB when ventilation rate was increased to 5 ACH, comprising Simulation 3 (BPB at 5 ACH);
3. Set 3 (U-Value Modification): Assessed the thermal impact of replacing the BPB's internal air cavities with EPS insulation at 5 ACH, comprising Simulation 4 (BPB + EPS at 5 ACH);
4. Set 4 (Cross-Examination): Compared all three wall assemblies under ventilation rates up to 10 ACH, comprising Simulation 5 (CHB at 10 ACH), Simulation 6 (BPB at 10 ACH), and Simulation 7 (BPB + EPS at 10 ACH), confirming the relative influence of envelope stratigraphy versus airflow across all tested systems.

2.4.7. Data Extraction and Post-Processing

Simulation Outputs

Performance data from the seven simulation runs were extracted using the VistaPro application within IESVE and exported to Microsoft Excel (Microsoft Corporation, Redmond, WA, USA) for post-processing. Three primary environmental parameters were recorded for the thermal zone: air temperature, operative temperature, and relative humidity. Data points were logged at 10-min intervals throughout the annual simulation period, yielding 52,560 discrete values per parameter for each scenario. These high-resolution datasets were subsequently averaged into 8760 hourly values and 365 daily values to facilitate comparative analysis against the outdoor environmental conditions defined in the EPW weather file.

Temperature and Frequency Analysis

Initial evaluations focused on tracking overall air temperature trends. Frequency distribution charts were generated by calculating the maximum and minimum hourly average air temperatures for each scenario and organizing the 8760 hourly data points into specific temperature bins (e.g., 27–28 °C). This binning process allowed for the calculation of percentage distributions and cumulative frequencies, clearly identifying the dominant indoor temperature ranges for each wall assembly.

Adaptive Thermal Comfort Evaluation

Because the modeled residential units are naturally ventilated, thermal performance was assessed using the Adaptive Comfort Model defined in ASHRAE Standard 55 [50]. This model operates on the principle that occupants in naturally ventilated spaces adapt to their local climate, resulting in a broader acceptable comfort range between 17 °C and 31 °C compared to mechanically conditioned buildings [51].

The monthly average outdoor temperature ($T_{outdoor,\ monthly\ average}$) was used to establish the baseline comfort temperature ($T_{comfort}$) using the standard's empirical formula:

$$T_{comfort} = 0.31 \times T_{outdoor,\ monthly\ average} + 17.8\ [^{\circ}C] \quad (1)$$

$$80\%\ acceptability\ Upper\ range = (0.31 * T_{outdoor,\ monthly\ average}) + 21.3\ [^{\circ}C] \quad (2)$$

$$80\%\ acceptability\ Lower\ range = (0.31 * T_{outdoor,\ monthly\ average}) + 14.3\ [^{\circ}C] \quad (3)$$

$$90\%\ acceptability\ Upper\ range = (0.31 * T_{outdoor,\ monthly\ average}) + 20.3\ [^{\circ}C] \quad (4)$$

$$90\%\ acceptability\ Lower\ range = (0.31 * T_{outdoor,\ monthly\ average}) + 15.3\ [^{\circ}C] \quad (5)$$

For this study, the 80% acceptability bounds (±3.5 °C variance from $T_{comfort}$) were used as the primary metric, while the 90% bounds (±2.5 °C) were recorded for supplementary observation as specified by the standard (Table 4). A logical function was applied to

evaluate all 8760 hourly operative temperatures for each simulation against the calculated monthly boundaries, counting the total annual hours within this acceptable comfort range.

Table 4. Calculated monthly comfort temperatures ($T_{comfort}$) and corresponding 80% and 90% acceptability limits for the BaSECo climate, derived from ASHRAE Standard 55 [50].

Month	$T_{outdoor,monthly\ average}$ *	Acceptability Upper Limits		$T_{comfort}$	Acceptability Lower Limits	
		80%	90%		90%	80%
	[°C]	[°C]	[°C]	[°C]	[°C]	[°C]
January	26.53	29.5	28.5	26.02	23.5	22.5
February	27.25	29.7	28.7	26.25	23.7	22.7
March	28.64	30.2	29.2	26.68	24.2	23.2
April	30.02	30.6	29.6	27.11	24.6	23.6
May	30.40	30.7	29.7	27.22	24.7	23.7
June	29.55	30.5	29.5	26.96	24.5	23.5
July	28.43	30.1	29.1	26.61	24.1	23.1
August	28.29	30.1	29.1	26.57	24.1	23.1
September	28.13	30.0	29.0	26.52	24.0	23.0
October	28.42	30.1	29.1	26.61	24.1	23.1
November	28.25	30.1	29.1	26.56	24.1	23.1
December	27.52	29.8	28.8	26.33	23.8	22.8

* Monthly average outdoor temperatures derived from the Manila NCR EPW climate file [3].

Relative Humidity Analysis

Indoor thermal comfort and air quality are significantly influenced by moisture levels, particularly relevant in Manila's tropical climate where ambient humidity frequently approaches 100%. Relative humidity (RH) records for each simulation were exported at 10-min intervals and processed into 8760 hourly averages. These indoor values, along with the hourly average air temperatures, were plotted against the outdoor baseline data extracted from the EPW weather file for comparative analysis.

A stringent composite comfort band of 40–60% RH was established by cross-referencing two international standards. The World Health Organization recommends an acceptable RH range of 40% to 70% to mitigate respiratory issues and mold development [52], while ASHRAE Standard 55 defines a range of 30% to 60% [50]. The adopted band of 40–60% takes the higher lower limit from WHO and the lower upper limit from ASHRAE, producing the most conservative threshold that simultaneously satisfies both standards. A logical function was applied to evaluate each hourly average against this threshold, quantifying the total annual hours each simulation scenario successfully maintained humidity within the healthy range.

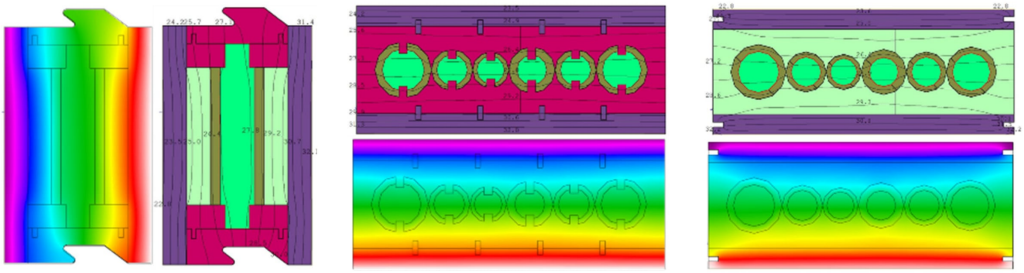
3. Results

3.1. Steady-State Thermal Analysis

Two-dimensional steady-state heat transfer through the BPB was evaluated using THERM (Version 7.8). Simulations were conducted across six distinct cross-sections representing single-brick configurations (A-A, B-B, C-C) and brick-to-brick connections (D-D, E-E, F-F). Performance was analyzed under diurnal and nocturnal conditions for both summer (21 June) and winter (21 December) design days. The full ranges of resulting thermal transmittances (U-values), internal surface temperatures, and peak heat flow rates are summarized in Table 5. To illustrate the maximum thermal bridging effects, the thermal gradients for peak summer daytime conditions are shown in Figures 11 and 12.

Table 5. Steady-state thermal properties of the six BPB cross-sections across all tested seasonal boundary conditions, derived from THERM finite-element analysis [41]. Peak heat flow values correspond to maximum thermal stress conditions (21 June, 12:00).

Cross-Section	Identifier	U-Value Range W/(m^2.K)	Average Indoor Surface Temp °C	Peak Heat Flow W
Single Brick	A-A	0.98–0.99	22.5	4.17
	B-B	1.10–1.25	23.0	6.90
	C-C	1.10–1.30	22.5	7.00
Brick-to-Brick	D-D	1.01–1.02	22.5	8.10
	E-E	1.09–1.27	22.9–23.5	11.75
	F-F	1.17–1.30	22.9–23.5	12.60



(**a**) (**b**) (**c**)

Figure 11. Steady-state thermal gradients generated in THERM under peak summer daytime conditions (21 June at 12:00), showing the heat flow distribution across single-brick cross-sections: (**a**) A-A, (**b**) B-B, and (**c**) C-C. The color-flooded views show the temperature field, from the exterior temperature of 32.5 °C (red) to the interior setpoint of 22 °C (blue). The other views show the cross-section geometry, with each material in its THERM color: purple for the ply-bamboo boards, olive green for the bamboo culms, magenta for the recycled plastic frame, and bright green for the air cavities.

Thermal Transmittance and Bridging Effects

The single-brick cross-sections established the following thermal performance baselines. Section A-A maintained a consistent U-value between 0.98 W/(m^2.K) and 0.99 W/(m^2.K) across all seasonal conditions, demonstrating stable thermal transmittance regardless of exterior temperature variation. Full seasonal heat flow values of A-A range from 2.16 W during summer nights to 4.17 W during summer days, and from 2.44 W to 3.12 W across winter conditions. Sections B-B and C-C, which incorporate larger proportions of the internal air cavity and plastic framing, showed U-values ranging between 1.1 W/(m^2.K) and 1.3 W/(m^2.K). The observed diurnal variation in U-values across these sections reflects the influence of changing temperature differentials on the thermal behavior of internal air cavities, with slightly higher transmittance recorded during nocturnal conditions. Peak summer daytime heat flows for B-B and C-C reached up to 6.9 W and 7.0 W, respectively. The indoor surface temperature averaged approximately 22.5 °C to 23.0 °C across all single-brick sections (Figure 11).

Connections between adjacent BPB units yielded higher thermal transmittances than the isolated single-brick sections. The solid-to-solid connection at Section D-D maintained a U-value of approximately 1.02 W/(m^2.K) with an indoor surface temperature of 22.5 °C. Peak summer daytime heat flow reached 8.1 W, reducing to 6.0 W and 4.7 W during winter day and night conditions, respectively. Section E-E (the plastic-to-bamboo connection) and Section F-F (the bamboo-to-air cavity connection) exhibited higher U-values, reaching up to 1.27 W/(m^2.K) and 1.30 W/(m^2.K), respectively. Notably, Section F-F exhibited a reverse diurnal pattern, with higher U-values recorded at night than during the day,

attributable to the reduced temperature differential altering the convective behavior of the bamboo-to-air-cavity interface. Section F-F recorded the highest overall heat flow of 12.6 W during the summer day, with internal surface temperatures at connection points ranging between 22.9 °C and 23.5 °C (Figure 12).

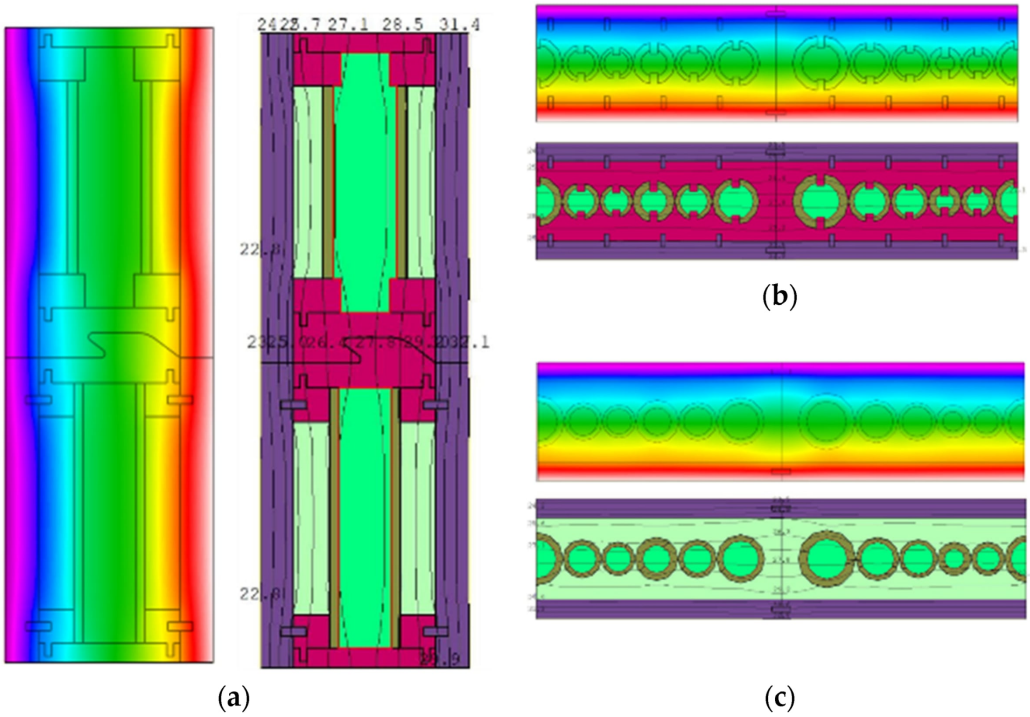


Figure 12. Steady-state thermal gradients generated in THERM under peak summer daytime conditions (21 June at 12:00), showing localized thermal bridging at brick-to-brick connection cross-sections: (**a**) D-D, (**b**) E-E, and (**c**) F-F. Elevated heat flux concentrations at the plastic-to-bamboo and bamboo-to-air cavity interfaces indicate the primary thermal bridge pathways. The color-flooded views show the temperature field, from the exterior temperature of 32.5 °C (red) to the interior setpoint of 22 °C (blue). The other views show the cross-section geometry. Each material appears in its THERM color: purple for the ply-bamboo boards, olive green for the bamboo culms, magenta for the recycled plastic frame, and bright green for the air cavities. Numbers in the geometry views are isotherm temperatures (°C) labeled by THERM.

3.2. Dynamic Hygrothermal Analysis (WUFI)

Dynamic hygrothermal simulations were conducted to evaluate moisture transfer and mold growth risk within the BPB under tropical climatic conditions. Performance was assessed by tracking surface temperature, relative humidity (RH), total water content, and localized mold indices over a one-year simulation period.

3.2.1. Annual Moisture and Surface Conditions

The annual hygrothermal conditions of the BPB exterior and interior surfaces are shown in Figure 13. The exterior surface exhibited distinct seasonal fluctuations, with temperatures ranging from a minimum of 23 °C (November to February) to a peak of 34 °C (April to July). Exterior relative humidity displayed daily cyclical trends but increased significantly from June through October, frequently reaching 100%. By contrast, the interior surface maintained a highly stable hygrothermal environment, with temperatures ranging from 25 °C to 26 °C and relative humidity consistently maintained between 62–65%. Total water content within the brick assembly followed a seasonal pattern, decreasing from February to June before rising again through October (Figure 13c). Despite these

fluctuations, the total mass of water remained within 8.4 kg/m^2 and 9.8 kg/m^2 throughout the annual cycle.

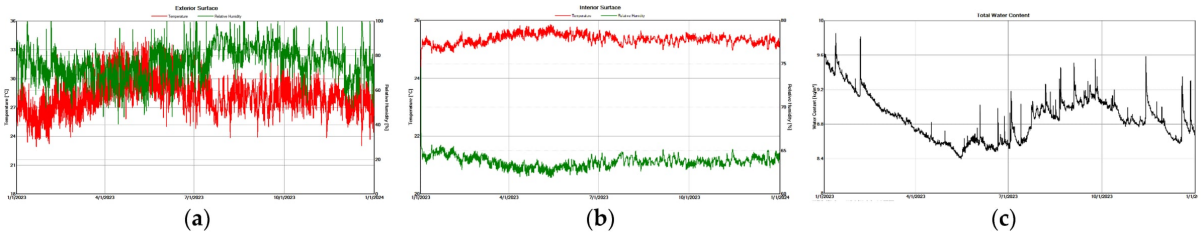


Figure 13. Annual hygrothermal performance of the BPB wall assembly simulated in WUFI® Pro over a one-year period: (**a**) exterior surface temperature (red) and relative humidity (green) showing seasonal fluctuations and monsoon peaks; (**b**) interior surface temperature (red) and relative humidity (green) demonstrating stable hygrothermal conditions throughout the year; (**c**) total water content of the brick assembly showing seasonal accumulation and drying cycles.

Hygrothermal conditions were further evaluated using isopleth charts plotting timestep data against established mold growth threshold curves (Figure 14). Each data point represents the simultaneous temperature and relative humidity recorded at a specific timestep, with lighter colors indicating earlier time steps and progressively darker colors indicating later points in the simulation year. The exterior surface data points, characterized by temperatures between 23 °C and 34 °C and relative humidity mainly between 60% and 100%, scattered widely above both limiting isopleths due to direct weather exposure. By contrast, the interior surface coordinates, bounded between 25 °C and 26 °C and 62% and 65% RH, remained entirely below both LIM B I (bio-utilizable substrates) and LIM B II (porous substrates such as bamboo and wood) [53]. This confirms that the interior space-facing surface of the BPB remains below the critical temperature and humidity threshold for mold growth throughout the year.

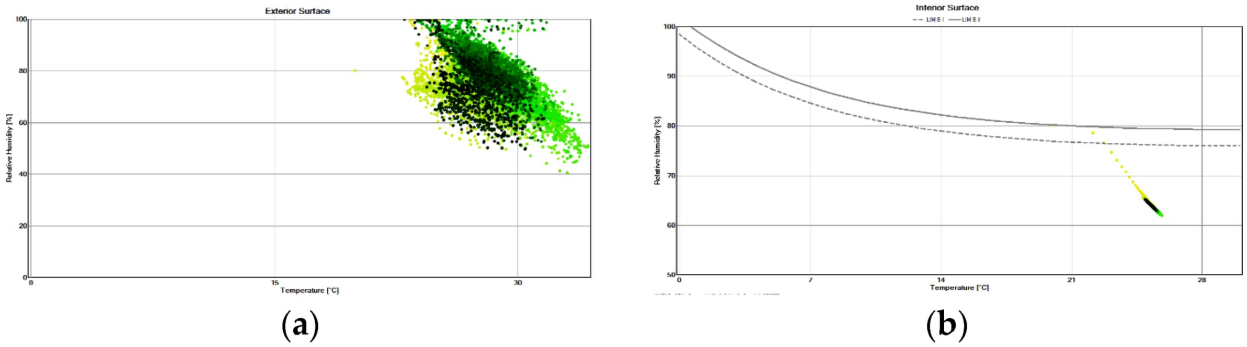


Figure 14. Isopleth charts generated using WUFI® Bio, plotting simulated annual temperature and relative humidity data points for the BPB (**a**) exterior and (**b**) interior surfaces against Sedlbauer's mold growth limiting isopleths (LIM B I and LIM B II) [53]. The isopleths are not drawn in (**a**), but they are identical to those in (**b**). Lighter points represent earlier time steps; darker points represent later time steps in the simulation year.

3.2.2. Localized Mold Risk Assessment

Moisture accumulation and mold growth probability were tracked across four specific cross-sections within the bamboo boards: the outer and inner faces of the exterior board (CS 1 and CS 2), and the cavity-facing and space-facing sides of the interior board (CS 3 and CS 4). The resulting peak moisture values and mold indices are summarized in Table 6.

Table 6. Peak hygrothermal metrics across the four evaluated BPB board cross-sections over a one-year simulation period. Mold indices are evaluated using the Viitanen model [45].

Monitoring Point	Location Description	Water Content Behavior	Peak MI
CS 1	Exterior board, outer face	Consistently exceeded near-zero MI for first half, linear increase to peak in second half	4.50
CS 2	Exterior board, inner face	Exceeded during first and final thirds; below threshold mid-year	0.15
CS 3	Interior board, cavity-facing	Exceeded threshold; peak in first half, decreasing toward threshold by year end	1.00
CS 4	Interior board, space-facing	Remained below critical threshold throughout	0.00

The outermost surface (CS 1) experienced the most severe weathering, with water content consistently exceeding the critical threshold throughout the year. The Mould Index maintained near-zero values during the first half of the year before increasing linearly through the second half, reaching 4.5 by the end of the annual cycle. The inner face of the exterior board (CS 2) displayed moderate moisture retention, with water content exceeding the critical threshold during the first and final thirds of the year while falling below it mid-year. Two distinct mold growth periods were recorded, with peak index of 0.15 and a secondary stable trend around 0.08, respectively. The internal cavity-facing layer (CS 3) showed a peak water content of approximately 243 kg/m^3 during the first half of the year, gradually decreasing toward the threshold value. The Mould Index grew slowly throughout the year, reaching a maximum of approximately 1.0 by year end. Most critically, the space-facing interior surface (CS 4) maintained a moisture content of approximately 177 kg/m^3, well below the 195 kg/m^3 critical limit, resulting in a sustained Mould Index of zero throughout the simulation.

3.3. Dynamic Thermal Zone Simulation (IESVE)

Dynamic thermal simulations were conducted on the reference single-zone model to evaluate the envelope-scale performance of the BPB against the CHB baseline. Because Manila's tropical climate exhibits negligible seasonal variation, performance was analyzed continuously across the 8760-h annual cycle. The simulations evaluated the interacting effects of envelope thermal mass, U-value enhancements through insulation, and natural ventilation rates (1, 5, and 10 ACH) on indoor air temperature, adaptive thermal comfort, and relative humidity. A comprehensive summary of the annual performance metrics across all seven simulation scenarios is provided in Table 7.

Table 7. Annual dynamic thermal zone simulation results comparing the BPB and CHB envelope systems across varying ventilation rates. The table details indoor temperature ranges, ASHRAE 55 adaptive comfort hours, and optimal relative humidity hours.

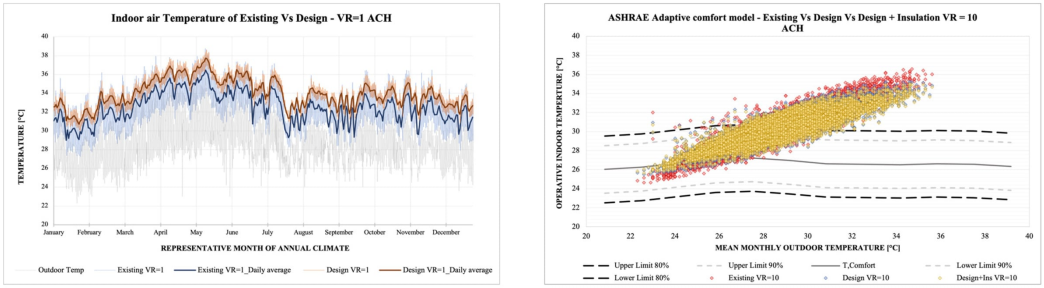
Scenario	Envelope System	Vent. Rate	Indoor Temp Range (°C)	ASHRAE 80% Comfort (h)	Optimal RH 40–60% (h)
Sim 1	Existing (CHB)	1 ACH	27.0–>38.0	1140 (13.0%)	2540 (29.0%)
Sim 2	Design (BPB)	1 ACH	29.9–38.5	0 (0.0%)	4345 (49.6%)
Sim 3	Design (BPB)	5 ACH	26.6–36.0	2050 (23.4%)	1951 (22.2%)

Table 7. *Cont.*

Scenario	Envelope System	Vent. Rate	Indoor Temp Range (°C)	ASHRAE 80% Comfort (h)	Optimal RH 40–60% (h)
Sim 4	Design (BPB + Ins)	5 ACH	26.8–35.8	1749 (19.9%)	~1900 (21.6%)
Sim 5	Existing (CHB)	10 ACH	24.4–36.4	~4380 (50.0%)	1446 (16.5%)
Sim 6	Design (BPB)	10 ACH	25.0–35.5	~4380 (50.0%)	1205 (13.7%)
Sim 7	Design (BPB + Ins)	10 ACH	25.2–35.1	~4380 (50.0%)	1154 (13.1%)

3.3.1. Envelope Thermal Dynamics and Insulation Performance

Baseline comparisons at 1 ACH revealed that the BPB significantly alters indoor thermal behavior compared to the CHB system. While both systems resulted in indoor temperatures higher than outdoor ambient conditions, the BPB effectively dampened diurnal temperature fluctuations (Figure 15a). The existing CHB wall exhibited a wide temperature bandwidth, with peak temperatures frequently exceeding 38 °C and a most frequent temperature range of 32–33 °C accounting for 17% of annual hours; 86.6% of annual hours recorded temperatures below 35 °C. The BPB reduced the daily temperature swing, with a most frequent range of 33–34 °C (24.7% of hours) and 87.4% of hours below 36 °C. However, this dampening effect also caused the BPB to retain heat during the night, resulting in an average annual indoor temperature 1.5 °C higher than the CHB baseline. This heat trap phenomenon explains a counterintuitive finding: the CHB recorded 1140 adaptive comfort hours (13%) at 1 ACH while the BPB recorded zero. The CHB's high U-value allows rapid nocturnal heat dissipation that briefly brings indoor temperatures within the comfort zone, whereas the BPB's lower U-value, while moderating peak temperatures, prevents the same nocturnal cooling.



(**a**) (**b**)

Figure 15. Dynamic thermal behavior of the building envelope across simulation scenarios. (**a**) Hourly indoor air temperature comparison at 1 ACH: CHB (Existing) data shown in blue tones (hourly: light blue; daily average: dark blue), and BPB (Design) data shown in orange-brown tones (hourly: light orange; daily average: dark brown), with outdoor temperature shown in grey, demonstrating the thermal dampening and heat trap effect of the BPB against the CHB baseline. (**b**) ASHRAE 55 adaptive comfort evaluation at 10 ACH: Existing CHB shown as red markers, Design BPB as blue markers, and Design BPB + Insulation as yellow markers, plotted against the 80% acceptability limits (black dashed lines), 90% acceptability limits (grey dashed lines), and comfort temperature $T_{Comfort}$ (solid grey line), illustrating the dominance of natural ventilation in achieving thermal acceptability regardless of envelope stratigraphy.

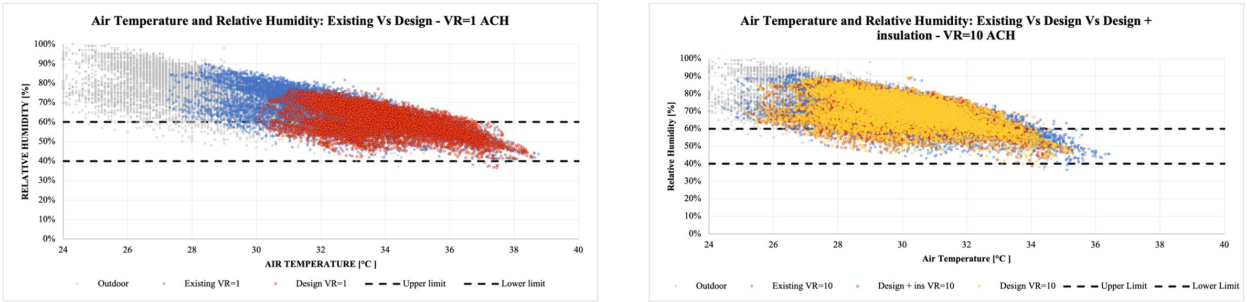
To isolate the impact of thermal transmittance, the standard BPB was compared against the insulated variant (BPB + EPS), representing a 38% reduction in U-value to 0.48 $W/(m^2.K)$. Under identical 5 ACH and 10 ACH conditions, the insulated wall produced negligible changes in indoor air temperature. At 5 ACH, both variants recorded a most frequent temperature range of 30–31 °C with approximately 87% of annual hours below 33 °C. The insulated envelope resulted in a slight comfort penalty; it reduced the

total adaptive comfort hours from 2050 to 1749. This indicates that in consistently hot tropical climates, adding insulation to a naturally ventilated space prevents the dissipation of internal heat gains.

3.3.2. The Natural Ventilation and Humidity Trade-Off

Operative thermal comfort, evaluated against the ASHRAE 55 80% acceptability limits [50], was found to be heavily dependent on air-exchange rate rather than envelope material. At 1 ACH, the BPB's heat retention resulted in zero annual hours within the adaptive comfort zone. Increasing the ventilation rate to 5 ACH dropped the daily average temperature by 2.5 °C and yielded 2050 comfort hours (23.4% of the year), with the most frequent temperature range dropping from 33–34 °C to 30–31 °C. Maximizing natural ventilation to 10 ACH resulted in all tested envelope systems achieving adaptive thermal comfort for approximately 50% of the year, with daily average temperatures closely mirroring outdoor conditions (Figure 15b). At 10 ACH, the most frequent temperature bin for all assemblies converged to 29–30 °C, confirming that at sufficient ventilation rates, envelope stratigraphy becomes the secondary performance driver.

While high ventilation rates resolved the thermal comfort deficit, they created a critical hygrothermal penalty. At 1 ACH, the BPB demonstrated exceptional moisture buffering, maintaining indoor RH within the optimal 40–60% band for 4345 h (49.6% of the year), significantly outperforming the CHB baseline of 2540 h (29.0%). The maximum indoor RH recorded under BPB was 77%, compared to 90% for CHB. As ventilation increased to 5 ACH, the interior was progressively flooded with Manila's naturally humid ambient air, reducing BPB comfort hours to 1951 (22.2%). At 10 ACH, all three envelope assemblies converged toward similar RH performance of approximately 69% annual average, with BPB recording only 1154–1205 comfortable RH hours and CHB recording 1446 h (Figure 16). This convergence reveals a critical operational trade-off in tropical passive design: maximizing thermal comfort through natural ventilation inherently compromises indoor humidity control, as the outdoor air used for cooling is itself highly saturated.



(**a**) (**b**)

Figure 16. Indoor air temperature and relative humidity scatter plots across simulation scenarios, with the RH comfort band (40–60%) indicated by black dashed lines and outdoor reference conditions shown in grey markers. (**a**) CHB vs. BPB at 1 ACH: Existing CHB shown in blue markers and Design BPB shown in red markers, demonstrating the moisture buffering superiority of the BPB and the reduction in annual RH range. (**b**) CHB, BPB, and BPB + Insulation at 10 ACH: Existing CHB shown in blue markers, Design BPB shown in yellow markers, and Design BPB + Insulation shown in red markers, demonstrating convergence of RH performance across all envelope systems under high-natural-ventilation conditions.

4. Discussion

The multi-scalar computational assessment conducted in this study evaluated the BPB across three distinct analytical scales: steady-state thermal bridging at the brick and

connection scale (THERM), dynamic hygrothermal transfer through the wall cross-section (WUFI), and indoor thermal comfort and humidity at the residential unit scale (IESVE). Collectively, the results reveal a system with strong hygrothermal credentials at the wall scale but with indoor thermal comfort heavily conditioned by passive ventilation strategy rather than envelope material choice. The following discussion interprets these findings across four interconnected themes: thermal bridging behavior at connections; moisture buffering and hygrothermal resilience; the heat trap phenomenon and the dominance of ventilation; and the fundamental ventilation–humidity trade-off inherent to tropical passive design.

4.1. Thermal Bridging and Steady-State Heat Transfer

The steady-state analysis revealed that while the core BPB provides adequate thermal resistance, its complex geometry introduces notable thermal bridging at connections. At the isolated single-brick scale, the natural cylindrical form and fibre structure of the bamboo culm effectively mitigated heat transmission, reducing localized heat transfer by up to 2 °C compared to simplified planar cross-sections. Interior surface temperatures remained consistently within the Philippine thermal comfort range of 22–26 °C [39], confirming the BPB's steady-state thermal adequacy.

Internal air cavities acted as effective insulators under high daytime temperature differentials (ΔT). However, as the ΔT fluctuates diurnally, sections containing high volumes of 3D-printed plastic and air cavities exhibit U-value variations between daytime and nocturnal conditions. While internal air cavities insulate effectively during high daytime ΔT, they inherently trap heat. This behavior was particularly pronounced in sections B-B and C-C, where air cavities account for most of the cross-sectional area.

At the brick-to-brick connection scale, structural interfaces between adjacent units increased localized heat flow by up to 80% compared to isolated single-brick sections, generating irregular isothermal patterns at the plastic-to-plyboard and plastic-to-plastic interfaces. These findings are consistent with established thermal bridge analysis in masonry and timber connections [26], confirming that irregular joinery geometries represent the primary thermal weakness in bamboo-based assemblies [27]. To mitigate these pathways in future physical deployment, targeted thermal breaks at connection points such as rubber gaskets or thin EPS inserts, distinct from the full cavity insulation tested in the IESVE simulations, would reduce conductive pathways at these vulnerable interfaces.

4.2. Moisture Buffering and Hygrothermal Resilience

Under dynamic tropical weathering, the BPB demonstrated a highly effective gradient of hygrothermal defense. The simulation confirms that the exterior bamboo board acts as a sacrificial weathering shield, absorbing intense seasonal rainfall peaking from June to October and routinely exceeding critical moisture thresholds, culminating in inevitable exterior mold growth. These findings align with hygrothermal analyses of bamboo building envelopes reported in the literature [16], confirming the material's layered capacity to moderate interior moisture conditions even under extreme tropical exposure.

Despite the exterior facing near 100% relative humidity during the monsoon season, the system's internal stratigraphy acted as an exceptional hygrothermal buffer. The interior ply-bamboo board maintained a highly stable environment of approximately 25 °C to 26 °C and 62–65% RH throughout the annual cycle. The exceptional moisture resistance of the interior board is primarily attributable to the high water vapour diffusion resistance factor of ply-bamboo, discussed in detail in Section 4.4. Because the interior moisture content remained strictly below the critical threshold of 195 kg/m^3, the space-facing Mould Index remained permanently at zero.

This confirms the short-term hygrothermal viability of the multi-layered BPB assembly in preventing indoor bio-contamination under the modeled annual conditions, provided the exterior ply-bamboo board is treated with weatherproofing agents or designed for periodic replacement. Long-term viability under sustained tropical exposure requires multi-year experimental validation beyond the scope of the present study.

4.3. The Thermal Mass Heat Trap and the Dominance of Ventilation

The single-zone dynamic simulations exposed a critical behavioral difference between the CHB and the BPB envelopes. The high U-value of the existing CHB allows rapid daytime heat gain but equally allows rapid nocturnal heat dissipation, briefly pulling indoor temperatures into the adaptive comfort zone. By contrast, the BPB acts as a thermal dampener. Its lower thermal transmittance narrows the daily temperature swing but simultaneously slows the release of internal heat, creating a heat trap effect within the building mass [54]. This mechanism explains the counterintuitive finding that the CHB recorded 1140 adaptive comfort hours (13%) at 1 ACH while the BPB recorded zero.

It is important to note that CHB's comfort hours at 1 ACH do not indicate superior thermal performance, as they result from larger nocturnal temperature drops rather than better thermal performance. The BPB's heat trap effect, while reducing comfort hours at low ventilation, narrows the daily temperature swing and provides superior humidity buffering. This demonstrates that comfort hours alone are an insufficient single metric for evaluating envelope performance in tropical climates, and that the BPB's thermal advantages are only fully realized when paired with adequate natural ventilation.

This heat trap phenomenon dictates that thermal comfort in the BPB system cannot rely on envelope physics alone. It is instead dependent on convective heat flushing via natural ventilation [55]. This finding reinforces the established principle in tropical building physics that passive ventilation strategies represent the primary determinant of indoor thermal comfort in non-conditioned buildings [55]. When ventilation was restricted to 1 ACH, trapped heat resulted in zero adaptive comfort hours for BPB. Increasing ventilation to 5 ACH dropped the daily average temperature by 2.5 °C, yielding 2050 comfort hours (23.4% of the year). Maximizing ventilation to 10 ACH completely overrode the envelope material properties, with all tested assemblies achieving approximately 50% comfort hours regardless of stratigraphy. This finding is consistent with a systematic review of bamboo-based envelope performance in hot and humid tropical climates, which similarly identifies ventilation as the primary comfort driver in naturally ventilated informal dwellings [17].

Furthermore, reducing the BPB U-value by 38% through EPS insulation substitution yielded minimal changes in indoor temperature under both 5 ACH and 10 ACH conditions. This confirms that in naturally ventilated tropical buildings, passive ventilation strategies far outweigh conductive insulation as a thermal comfort driver. The practical implication is significant: investment in envelope insulation alone is insufficient in this climate. Prioritizing cross-ventilation design, window placement, and airflow pathways will deliver substantially greater comfort improvements than material U-value enhancements.

4.4. The Ventilation–Humidity Trade-Off

While maximizing natural ventilation resolves the heat trap, it introduces a severe hygrothermal penalty. At low ventilation rates, the BPB exhibits outstanding internal humidity control. This performance is primarily attributable to the exceptionally high water vapour diffusion resistance factor (μ-value) of the interior ply-bamboo boards, recorded at 1392.8 [37,38]. This high μ-value effectively resists the diffusion of outdoor moisture through the wall assembly, maintaining indoor relative humidity within the optimal 40–60% band for 4345 h (49.6% of the year) at 1 ACH.

However, as the ventilation rate was increased to flush out sensible heat gains, the indoor environment was progressively saturated with Manila's naturally humid outdoor air. At 5 ACH, optimal RH hours dropped to 1951 (22.2% of the year). At 10 ACH, all three envelope assemblies converged toward similar RH performance of approximately 69% annual average, with optimal RH hours reducing further to approximately 1200 h regardless of wall stratigraphy. This convergence confirms that at high ventilation rates, the μ-value advantage of the ply-bamboo boards is overwhelmed by the volume of saturated outdoor air entering the space.

This exposes a fundamental operational conflict in tropical passive design. Maximizing thermal comfort through natural ventilation inherently compromises indoor humidity control, as the outdoor air used for cooling is itself highly saturated. The practical implication is that occupants of naturally ventilated BPB buildings in Manila face an unavoidable trade-off between thermal comfort and hygrothermal health conditions. Integrated passive design strategies, such as dehumidifying vegetation screens, thermal chimneys, or phase-change materials, may offer partial mitigation of this conflict and represent a critical direction for future research.

4.5. Methodological Limitations

While these simulations provide a robust comparative baseline, the abstraction of the BPB's complex 3D geometry into 1D and 2D computational layers represents a necessary simplification. The 3D-printed plastic components, which constitute a significant proportion of the brick's total volume, were homogenized as uniform thermal layers rather than modelled in their actual geometric configuration. This simplification was applied consistently across all simulation scales to maintain methodological coherence.

The single-zone model adopted a conservative Window-to-Wall Ratio of 4.0%, which may not physically support 10 ACH through natural ventilation alone in real BaSECo units. The 10 ACH scenario should therefore be interpreted as a best-case parametric condition rather than a guaranteed real-world outcome and requires validation through computational fluid dynamics (CFD) or physical airflow measurements.

The flat-layer abstraction of the cylindrical bamboo culms introduces a geometric simplification error in the calculated U-value and thermal mass. Standard hygrothermal simulation protocols are designed for planar orthogonal assemblies [24,25], requiring the curved bamboo geometry to be represented as equivalent flat layers. While this abstraction enables systematic comparison across envelope systems, it may underestimate localized thermal bridging and moisture infiltration at the culm-to-plastic interfaces. The magnitude of this error is difficult to quantify without full 3D finite-element validation. However, given that the performance differential between BPB and CHB is substantially large, with the BPB U-value approximately 60% lower than CHB, the principal comparative conclusions are unlikely to be reversed by this abstraction. Quantitative 3D validation remains a priority for future work.

The μ-value of 1392.8 adopted for the ply-bamboo boards exerts a critical influence on the interior mold growth results, as the water vapour diffusion resistance factor has been identified as the key parameter governing RH simulation outcomes in bamboo-based assemblies [37,38]. This property varies with bamboo species, moisture content, density, and manufacturing process, introducing inherent uncertainty in the modeled hygrothermal response. If the actual μ-value of the ply-bamboo boards in a fabricated assembly differs from the adopted value due to species variation or production conditions, the interior moisture buffering performance could differ from the simulated results. A formal sensitivity analysis of this parameter and physical measurement of the fabricated

BPB assembly's hygrothermal properties are therefore identified as priorities for future experimental validation.

The present study models a single annual hygrothermal cycle and does not account for the progressive degradation of the exterior bamboo board, which reached a Mould Index of 4.5 by year-end. In practice, fungal colonization of the exterior face would progressively alter the moisture storage function and vapour diffusion resistance of the outer board over multiple years, potentially reducing its buffering capacity and increasing moisture loads on the inner layers. This represents a significant limitation of the one-year simulation approach. Future work should incorporate multi-year degradation functions for bio-based materials in WUFI or investigate surface treatment strategies such as weatherproofing coatings or sacrificial cladding layers to protect the exterior board and maintain long-term system performance.

The IESVE single-zone simulations used the nominal U-value of the isolated BPB wall assembly (0.768 W/(m^2·K)) without incorporating the linear thermal transmittance contribution of the brick-to-brick connections identified in the THERM analysis. For a BPB module with a 600 × 400 mm wall face, horizontal joints (Section D-D) every 400 mm and vertical joints (Sections E-E and F-F) every 600 mm yield approximately 4 linear metres of joints per m^2 of wall area. Incorporating a conservative linear thermal transmittance estimate for these connections would increase the effective wall U-value above the nominal value, reducing but not eliminating the thermal performance advantage over CHB (1.921 W/(m^2·K)). This represents a methodological limitation. Future IESVE simulations should therefore incorporate ISO 14683 [56]compliant linear thermal transmittance corrections for the connection geometry.

Additionally, the thermal comfort assessment relies on the ASHRAE 55 adaptive comfort model, which evaluates operative temperature independently from relative humidity. This decoupled approach represents a known limitation in humid tropical climates where elevated RH significantly amplifies perceived heat stress beyond what temperature alone indicates. Integrated comfort metrics such as the Standard Effective Temperature (SET) or the Universal Thermal Climate Index (UTCI), which simultaneously account for temperature, humidity, and air movement, would provide a more comprehensive evaluation of occupant comfort in hot–humid contexts and are recommended for future work.

The present study evaluates short-term hygrothermal performance over a single annual simulation cycle and does not address the long-term durability of the bio-based components. Natural bamboo is susceptible to several degradation mechanisms in tropical humid climates, including fungal decay, biological attack from insects, wetting–drying cycle fatigue, UV weathering, and dimensional changes due to moisture absorption and desorption. These mechanisms could progressively alter the material's thermal conductivity, vapour diffusion resistance, and structural integrity over the service life of the assembly, potentially reducing the hygrothermal performance advantages demonstrated in the present study. The present study therefore demonstrates short-term hygrothermal performance potential rather than long-term durability or service-life performance, and should be interpreted accordingly.

Building upon the physical connector prototyping validated in a companion study [12], future research should prioritize full-scale hot-box thermal testing to validate these computational models under controlled physical conditions. Additionally, localized 3D finite-element thermal bridging simulations at the connection interfaces would provide a more precise characterization of the heat flow pathways identified in Section 4.1.

5. Conclusions

This study evaluated the dynamic thermal and hygrothermal performance of a novel Bamboo–Plastic Brick (BPB), designed as a sustainable building envelope for informal settlements in tropical climates like BaSECo, Manila. Using multi-scalar computational assessment (THERM, WUFI, and IESVE), the research quantified the physical behavior of the BPB assembly compared to prevalent Concrete Hollow Block (CHB) construction. The findings demonstrate that replacing conventional mineral-based materials with engineered bamboo and recycled plastic significantly alters the building physics of the envelope, presenting both critical advantages and specific operational trade-offs.

At the brick and wall cross-section scales, the BPB demonstrated exceptional hygrothermal resilience. The natural cylindrical form and fibrous structure of the bamboo culms provided superior localized thermal resistance, reducing heat transmission by up to 2 °C compared to simplified planar sections. While the exterior weathering face inevitably sustained moisture accumulation and mold growth during the monsoon season, the internal stratigraphy successfully buffered the interior space. The innermost surface maintained a stable environment well below the critical moisture threshold, yielding a zero Mould Index and confirming the system's viability for maintaining safe indoor air quality in highly humid environments.

At the residential unit scale, however, the BPB exhibited a pronounced heat trap effect. While the envelope dampened daily temperature spikes, its thermal mass slowed the release of internal heat at night. Dynamic simulations confirmed that supplemental insulation is ineffective in this context, and thermal comfort is entirely reliant on high natural ventilation rates. Maximizing ventilation to 10 ACH provided adaptive thermal comfort for 50% of the year across all tested envelope systems but inherently compromised the envelope's ability to regulate indoor humidity, revealing a fundamental operational trade-off in tropical passive design.

Ultimately, this research demonstrates that the BPB exhibits promising hygrothermal and thermal performance as an alternative to conventional CHB construction in tropical informal settlements, provided it is deployed with optimized passive ventilation strategies. Broader sustainability claims require further validation through physical hot-box testing, life-cycle assessment, embodied carbon quantification, economic feasibility analysis, fire performance testing, and long-term durability studies. Future work will prioritize full-scale hot-box thermal testing and field validation in an occupied BaSECo unit, building on the physical prototyping documented in a companion study [12]. Together with that companion study addressing digital fabrication workflow and community-embedded construction, these findings contribute to a holistic framework for climate-resilient informal housing in tropical contexts.

Author Contributions: L.F. and M.A. contributed equally to this work. Conceptualization, L.F. and M.A.; methodology, L.F. and M.A.; software, L.F. and M.A.; validation, L.F. and M.A.; formal analysis, L.F. and M.A.; investigation, L.F. and M.A.; resources, G.I.; data curation, L.F. and M.A.; writing—original draft preparation, L.F.; writing—review and editing, L.F., M.A. and G.I.; visualization, L.F. and M.A.; supervision, G.I.; project administration, L.F., M.A. and G.I. All authors have read and agreed to the published version of the manuscript.

Funding: This research received no external funding.

Data Availability Statement: The data presented in this study are available on request from the corresponding author.

Acknowledgments: This paper is based on the MSc thesis of L. Fahmy and M. Aboeloyoon, completed at Politecnico di Milano under the supervision of G. Iannaccone, P. Ruttico, and F. Rossini. The authors would like to express their sincere gratitude to Pierpaolo Ruttico for his invaluable guidance as thesis

co-supervisor and for facilitating the physical prototyping as head of IndexLab, and to the IndexLab team for their technical assistance during the fabrication process. We are deeply thankful to Francesco Pittau for generously providing the raw bamboo culms used for the physical prototypes. During the preparation of this manuscript, the authors used Gemini 3.1 Pro (Google DeepMind, London, UK) and Claude Sonnet 4.6 (Anthropic, San Francisco, CA, USA) for structural formatting and language refinement. The authors have reviewed and edited all AI-assisted output and take full responsibility for the content of this publication.

Conflicts of Interest: The authors declare no conflicts of interest. Prof. Giuliana Iannaccone is a Guest Editor for Buildings. To ensure the integrity of the peer-review process, she was entirely excluded from the editorial handling, reviewer selection, and final decision-making regarding this manuscript. The funders had no role in the design of the study; in the collection, analyses, or interpretation of data; in the writing of the manuscript; or in the decision to publish the results.

Abbreviations

The following abbreviations are used in this manuscript:

ACH	Air Changes per Hour
AM	Additive Manufacturing
ASHRAE	American Society of Heating, Refrigerating and Air-Conditioning Engineers
BPB	Bamboo–Plastic Brick
CFD	Computational Fluid Dynamics
CHB	Concrete Hollow Block
CIBSE	Chartered Institution of Building Services Engineers
DFab	Digital Fabrication
EN	European Norm
EPW	EnergyPlus Weather File
EPS	Expanded Polystyrene
HVAC	Heating, Ventilation and Air Conditioning
IESVE	Integrated Environmental Solutions Virtual Environment
ISO	International Organization for Standardization
LFAM	Large-Format Additive Manufacturing
LIM B I	Limiting Isopleth Mould: Bio-utilizable Substrates
LIM B II	Limiting Isopleth Mould: Porous Substrates
LBNL	Lawrence Berkeley National Laboratory
MI	Mould Index
NCR	National Capital Region
PET	Polyethylene Terephthalate
RH	Relative Humidity
R_{SI}	Internal Surface Thermal Resistance
R_{SE}	External Surface Thermal Resistance
THERM	Two-dimensional Heat Transfer software (LBNL)
WHO	World Health Organization
WUFI	Wärme und Feuchte Instationär (Heat and Moisture Transiently)
WTA	Scientific-Technical Association for Building Maintenance and Monument Preservation (Germany)
WWR	Window-to-Wall Ratio

Appendix A

A parametric script was developed in Grasshopper within Rhinoceros 3D (Version 7) to address THERM's limitations in natively meshing circular geometries. It used the open-source Ladybug (Version 0.0.69) and Honeybee (Version 0.0.66) plugins (Ladybug Tools LLC; available online: https://www.ladybug.tools). The script performed three sequential operations: first, it imported the bamboo culm cross-section geometry defined

by the average culm diameter and wall thickness; second, it discretized the circular profiles into high-resolution polygonal meshes approximating the curved geometry; and third, it exported the resulting cross-sections in a format compatible with the THERM finite-element environment. This parametric approach ensured consistency across all six tested cross-sections (A-A through F-F) and enabled systematic variation in culm diameter and wall thickness as input parameters. The visual programming workflow is shown in Figure A1.

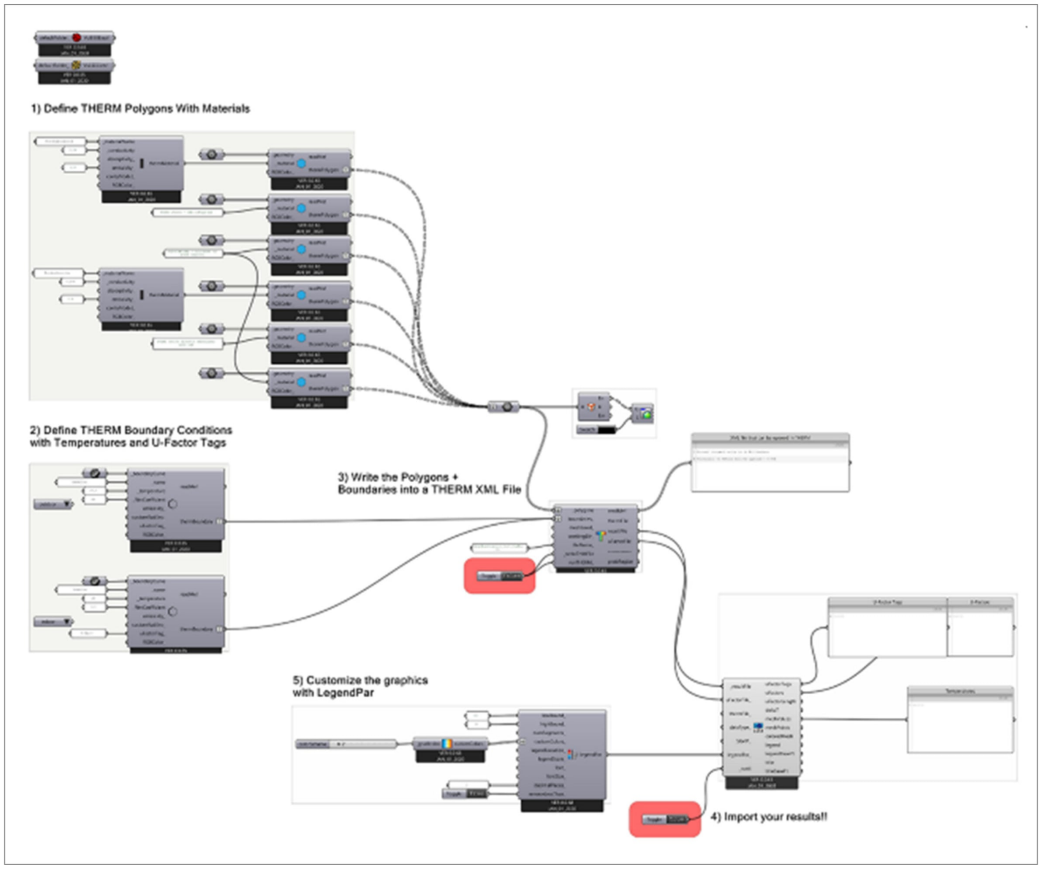


Figure A1. Parametric THERM modeling script developed in Grasshopper for Rhinoceros 3D, showing the sequential workflow for discretizing bamboo culm circular cross-sections into polygonal meshes for export to the THERM finite-element environment. Colors and symbols are those of the standard Grasshopper interface. Grey frames group the components of each workflow stage, labeled 1 to 5.

References

1. Galace, U.N. Housing Insecurity and Economic Development: A Case Study of Informal Settlements in Manila, Philippines. In *APISA 17th Annual Congress (APISA2023) Official Conference Proceedings*; The International Academic Forum: Nagoya, Japan, 2023; pp. 9–17. [CrossRef]
2. Asian Development Bank. *Poverty in the Philippines: Causes, Constraints and Opportunities*; Asian Development Bank: Manila, Philippines, 2009. Available online: https://www.adb.org/publications/poverty-philippines-causes-constraints-and-opportunities (accessed on 20 March 2026).
3. Climate.OneBuilding.org. Repository of Free Climate Data for Building Performance Simulation: Philippines, National Capital Region. Available online: https://climate.onebuilding.org/WMO_Region_5_Southwest_Pacific/PHL_Philippines/index.html#IDNCR_National_Capital_Region- (accessed on 18 May 2023).
4. UN-Habitat. *World Cities Report 2024: Cities and Climate Action*; United Nations Human Settlements Programme (UN-Habitat): Nairobi, Kenya, 2024. Available online: https://digitallibrary.un.org/record/4065171 (accessed on 20 March 2026).
5. Hugo, J.M.; Sonnendecker, P.W. Ground-Level Documentation of Heat Stress Exposure and Response Strategies in Informal Settlements in Tshwane, South Africa. *Smart Sustain. Built Environ.* **2024**, *13*, 1177–1193. [CrossRef]

6. Rossini, F. Urban Design and Informal Settlements: Placemaking Activities and Temporary Architectural Interventions in BaSECo Compound. *Urban Des. Int.* **2021**, *29*, 4–24. [CrossRef]
7. Ouedraogo, A.L.S.-N.; Hema, C.; N'guiro, S.M.; Nshimiyimana, P.; Messan, A. Optimisation of Thermal Comfort of Building in a Hot and Dry Tropical Climate: A Comparative Approach between Compressed Earth/Concrete Block Envelopes. *J. Miner. Mater. Charact. Eng.* **2024**, *12*, 1–16. [CrossRef]
8. Hens, H.S. *Building Physics—Heat, Air and Moisture: Fundamentals and Engineering Methods with Examples and Exercises*; John Wiley & Sons: Hoboken, NJ, USA, 2017.
9. Kamel, E.; Habibi, S.; Memari, A.M. State of the Practice Review of Moisture Management in Residential Buildings through Sensors. *Structures* **2024**, *59*, 105698. [CrossRef]
10. United Nations Environment Programme. *Not Just Another Brick in the Wall: The Solutions Exist—Scaling Them Will Build on Progress and Cut Emissions Fast. Global Status Report for Buildings and Construction 2024/2025*; United Nations Environment Programme: Nairobi, Kenya, 2025. [CrossRef]
11. Inam, A. Cultural Homogenization and the Decline of Vernacular Architecture: Challenges and Opportunities. *Int. J. Multidiscip. Res.* **2025**, *7*, 39067. [CrossRef]
12. Ahmed, M.A.; Fahmy, L.; Ahmed, T.M.F. Socially Embedded Innovation: Digital Fabrication for Climate-Resilient Informal Housing. In *Proceedings of the 31st International Conference of the Association for Computer-Aided Architectural Design Research in Asia (CAADRIA) 2026*; CAADRIA: Hong Kong, China, 2026; Volume 2, pp. 71–80. Available online: https://papers.cumincad.org/data/works/att/caadria2026_600.pdf (accessed on 15 May 2026).
13. Chaowana, K.; Wisadsatorn, S.; Chaowana, P. Bamboo as a Sustainable Building Material—Culm Characteristics and Properties. *Sustainability* **2021**, *13*, 7376. [CrossRef]
14. Adier, M.F.V.; Sevilla, M.E.P.; Valerio, D.N.R.; Ongpeng, J.M.C. Bamboo as Sustainable Building Materials: A Systematic Review of Properties, Treatment Methods, and Standards. *Buildings* **2023**, *13*, 2449. [CrossRef]
15. Yadav, M.; Mathur, A. Bamboo as a Sustainable Material in the Construction Industry: An Overview. *Mater. Today Proc.* **2021**, *43*, 2872–2876. [CrossRef]
16. Li, H.; Yang, S.; Zha, Z.; Fei, B.; Wang, X. Hygrothermal Properties Analysis of Bamboo Building Envelope with Different Insulation Systems in Five Climate Zones. *Buildings* **2023**, *13*, 1214. [CrossRef]
17. Chen Austin, M.; Solano, T.; Carpino, C.; Castaño, C.; Mora, D. Performance Assessment Methods and Effects of Bamboo-Based Envelopes in Buildings Under Hot and Humid Conditions. In *Bamboo and Sustainable Construction*; Palombini, F.L., Nogueira, F.M., Eds.; Springer: Singapore, 2023; pp. 291–321. [CrossRef] [PubMed]
18. Galmarini, B.; Costa, P.; Chiesi, L. Natural Building Materials and Social Representations in Informal Settlements: How Perceptions of Bamboo Interfere with Sustainable, Affordable, and Quality Housing. *Sustainability* **2022**, *14*, 12252. [CrossRef]
19. Kadivar, M.; Gauss, C.; Ghavami, K.; Savastano, H. Densification of Bamboo: State of the Art. *Materials* **2020**, *13*, 4346. [CrossRef] [PubMed]
20. Gan, J.; Chen, M.; Semple, K.; Liu, X.; Dai, C.; Tu, Q. Life Cycle Assessment of Bamboo Products: Review and Harmonization. *Sci. Total Environ.* **2022**, *849*, 157937. [CrossRef] [PubMed]
21. Lao, W.; Hu, J.; Huang, Y.; Li, X. Environmental Footprints of Wood and Bamboo Reconstituted Materials Production in China: A Cradle-to-Gate Life Cycle Assessment. *Ind. Crops Prod.* **2025**, *232*, 121320. [CrossRef]
22. Chaowana, P. Bamboo: An Alternative Raw Material for Wood and Wood-Based Composites. *J. Mater. Sci. Res.* **2013**, *2*, 90–102. [CrossRef]
23. Trujillo, D.J.; López, L.F. Bamboo Material Characterisation. In *Nonconventional and Vernacular Construction Materials*; Elsevier: Amsterdam, The Netherlands, 2020; pp. 491–520. [CrossRef]
24. Lorenzo, R.; Lee, C.; Oliva-Salinas, J.G.; Ontiveros-Hernandez, M.J. BIM Bamboo: A Digital Design Framework for Bamboo Culms. *Proc. Inst. Civ. Eng.-Struct. Build.* **2017**, *170*, 295–302. [CrossRef]
25. Wissenschaftlich-Technische Arbeitsgemeinschaft für Bauwerkserhaltung und Denkmalpflege (WTA). *Simulation of Heat and Moisture Transfer*; WTA Guideline 6-2; WTA: Munich, Germany, 2014.
26. Theodosiou, T.G.; Papadopoulos, A.M. The Impact of Thermal Bridges on the Energy Demand of Buildings with Double Brick Wall Constructions. *Energy Build.* **2008**, *40*, 2083–2089. [CrossRef]
27. Janssen, J.J. *Designing and Building with Bamboo*; International Network for Bamboo and Rattan (INBAR): Beijing, China, 2000; pp. 130–133. ISBN 81-86247-46-7.
28. American Society of Heating, Refrigerating and Air-Conditioning Engineers (ASHRAE). *2021 ASHRAE Handbook—Fundamentals*; ASHRAE: Atlanta, GA, USA, 2021.
29. Wang, T.-H.; Espinosa Trujillo, O.; Chang, W.-S.; Deng, B. Encoding Bamboo's Nature for Freeform Structure Design. *Int. J. Archit. Comput.* **2017**, *15*, 169–182. [CrossRef]

30. Hauptman, J.; Hindman, D.; Hack, K.; Marggraf, G. Smart Bamboo Systems: Combining Material Intelligence with Modern Manufacturing. In Proceedings of the 19th International Conference on Non-Conventional Materials and Technologies (NOCMAT 2022), Virtually, 25 July 2022. [CrossRef]
31. World Bank Group. *Market Study for the Philippines: Plastics Circularity Opportunities and Barriers*; World Bank: Washington, DC, USA, 2021. Available online: http://documents.worldbank.org/curated/en/183811616083609678 (accessed on 20 March 2026).
32. Mao, J.; Hsu, L.; Altheeb, M.; Grigoriadis, K. Fused Space in Architecture via Multi-Material 3D Printing Using Recycled Plastic: Design, Fabrication, and Application. *Buildings* **2025**, *15*, 2588. [CrossRef]
33. Plastic Odyssey. Scaling Local Solutions to Solve the Global Plastic Crisis. Available online: https://plasticodyssey.org/ (accessed on 20 March 2026).
34. Koppe, J.C.; Saubke, D.; Redlich, T. Towards Circular Cities—The Dynamics of Supply Chains and Local Manufacturing. In *Proceedings of the Conference on Production Systems and Logistics: CPSL 2024*; Publish-Ing.: Hanover, Germany, 2024. [CrossRef] [PubMed]
35. Ünlü, E.; Sýsová, K.; Vele, J. Secret Factory: Networked Fabrication and Digital Maker Communities—Unlocking the Further Potential of Distributed 3D Printings. In *ARCHITECTURAL INFORMATICS—Proceedings of the 30th CAADRIA Conference, Tokyo, Japan, 22–29 March 2025*; Association for Computer-Aided Architectural Design Research in Asia (CAADRIA): Hong Kong, China, 2025; pp. 141–150. [CrossRef]
36. Sellami, I.; Amin, H.; Ozturk, O.; Zaman, A.; Sever, S.D.; Tok, E. Digital, Localised and Human-Centred Design Makerspaces: Nurturing Skills, Values and Global Citizenship for Sustainability. *Discov. Educ.* **2025**, *4*, 28. [CrossRef]
37. Huang, Z.; Künzel, H.; Krus, M.; Zhang, W. Three-Dimensional Tests on Hygric Properties of Laminated Bamboo and Bamboo Scrimber. *J. Build. Eng.* **2022**, *56*, 104712. [CrossRef]
38. Huang, Z.; Sun, Y.; Musso, F. Experimental Study on Bamboo Hygrothermal Properties and the Impact of Bamboo-Based Panel Process. *Constr. Build. Mater.* **2017**, *155*, 1112–1125. [CrossRef]
39. Andamon, M.M. Thermal Comfort in Philippine Office Buildings: The Coolth* Preference. In Proceedings of the 38th International Conference of Architectural Science Association (ANZAScA)—Contexts of Architecture, Launceston, TAS, Australia, 10–12 November 2004.
40. *ISO 10077-2:2017*; Thermal Performance of Windows, Doors and Shutters—Calculation of Thermal Transmittance—Part 2: Numerical Method for Frames. International Organization for Standardization (ISO): Geneva, Switzerland, 2017. Available online: https://www.iso.org/standard/64995.html (accessed on 3 June 2023).
41. Lawrence Berkeley National Laboratory. *THERM 7.8 Material Library*; Lawrence Berkeley National Laboratory (LBNL): Berkeley, CA, USA, 2021. Available online: https://windows.lbl.gov/software/therm (accessed on 27 May 2023).
42. *EN 15026:2007*; Hygrothermal Performance of Building Components and Building Elements—Assessment of Moisture Transfer by Numerical Simulation. European Committee for Standardization (CEN): Brussels, Belgium, 2007.
43. Holm, A.; Krus, M.; Künzel, H.M. Grenzen der Feuchtetransportberechnung bei Betonaußenbauteilen. *Tagungsband* **1999**, *5*, 405–414.
44. Krus, M. *Moisture Transport and Storage Coefficients of Porous Mineral Building Materials: Theoretical Principles and New Test Methods*; Fraunhofer IRB Verlag: Stuttgart, Germany, 1996.
45. Viitanen, H.; Ritschkoff, A.C. *Mould Growth in Pine and Spruce Sapwood in Relation to Air Humidity and Temperature*; Rapport Institutionen för Virkeslära No. 221; Department of Forest Products, Swedish University of Agricultural Sciences: Uppsala, Sweden, 1991.
46. Integrated Environmental Solutions (IES). *VE 2023 User Guide*; Integrated Environmental Solutions Limited: Glasgow, UK, 2023.
47. Integrated Environmental Solutions (IES). *ApacheSim Technical Analysis User Guide*; Integrated Environmental Solutions Limited: Glasgow, UK, 2023.
48. Chartered Institution of Building Services Engineers (CIBSE). *Guide A: Environmental Design*, 8th ed.; CIBSE: London, UK, 2015.
49. *ANSI/ASHRAE Standard 62.1-2013*; Ventilation for Acceptable Indoor Air Quality. American Society of Heating, Refrigerating and Air-Conditioning Engineers (ASHRAE): Atlanta, GA, USA, 2013. Available online: https://www.ashrae.org (accessed on 7 May 2023).
50. *ANSI/ASHRAE Standard 55-2004*; Thermal Environmental Conditions for Human Occupancy. American Society of Heating, Refrigerating and Air-Conditioning Engineers (ASHRAE): Atlanta, GA, USA, 2004.
51. Nicol, J.F.; Humphreys, M.A. Understanding the Adaptive Approach to Thermal Comfort. *ASHRAE Trans.* **1998**, *104*, 991–1004.
52. World Health Organization Regional Office for Europe (WHO). *WHO Guidelines for Indoor Air Quality: Dampness and Mould*; WHO Regional Office for Europe: Copenhagen, Denmark, 2009.
53. Sedlbauer, K. *Vorhersage von Schimmelpilzbildung auf und in Bauteilen*; Fraunhofer IRB Verlag: Stuttgart, Germany, 2001. [CrossRef]
54. Hart, G.H. K-Value, U-Value, R-Value, C-Value. Insulation Outlook. 1 March 2009. Available online: https://insulation.org/io/articles/k-value-u-value-r-value-c-value/ (accessed on 19 June 2023).

55. Blondeau, P.; Spérandio, M.; Allard, F. Night Ventilation for Building Cooling in Summer. *Sol. Energy* **1997**, *61*, 327–335. [CrossRef]
56. *Standard's ISO 14683:2017*; Thermal Bridges in Building Construction—Linear Thermal Transmittance—Simplified Methods and Default Values. International Organization for Standardization (ISO): Geneva, Switzerland, 2017.

Disclaimer/Publisher's Note: The statements, opinions and data contained in all publications are solely those of the individual author(s) and contributor(s) and not of MDPI and/or the editor(s). MDPI and/or the editor(s) disclaim responsibility for any injury to people or property resulting from any ideas, methods, instructions or products referred to in the content.